ARL-TR-9216 ● AUG 2021

DEVCOM ARMY RESEARCH LABORATORY

Investigation of Thermoelastic Damping in Microelectromechanical System (MEMS) Quadruple-Mass Gyroscope (QMG) Designs

by Alex Mazzoni, Ryan Rudy, Ryan Knight, and Jeff Pulskamp

Approved for public release: distribution unlimited.

NOTICES

Disclaimers

The findings in this report are not to be construed as an official Department of the Army position unless so designated by other authorized documents.

Citation of manufacturer's or trade names does not constitute an official endorsement or approval of the use thereof.

Destroy this report when it is no longer needed. Do not return it to the originator.

ARL-TR-9216 ● AUG 2021

Investigation of Thermoelastic Damping in Microelectromechanical System (MEMS) Quadruple-Mass Gyroscope (QMG) Designs

Alex Mazzoni
Oak Ridge Associated Universities

Ryan Rudy, Ryan Knight, and Jeff Pulskamp
Sensors and Electron Devices Directorate, DEVCOM Army Research Laboratory

Approved for public release: distribution unlimited.

REPORT DOCUMENTATION PAGE

Form Approved
OMB No. 0704-0188

Public reporting burden for this collection of information is estimated to average 1 hour per response, including the time for reviewing instructions, searching existing data sources, gathering and maintaining the data needed, and completing and reviewing the collection information. Send comments regarding this burden estimate or any other aspect of this collection of information, including suggestions for reducing the burden, to Department of Defense, Washington Headquarters Services, Directorate for Information Operations and Reports (0704-0188), 1215 Jefferson Davis Highway, Suite 1204, Arlington, VA 22202-4302. Respondents should be aware that notwithstanding any other provision of law, no person shall be subject to any penalty for failing to comply with a collection of information if it does not display a currently valid OMB control number.
PLEASE DO NOT RETURN YOUR FORM TO THE ABOVE ADDRESS.

1. REPORT DATE *(DD-MM-YYYY)*	2. REPORT TYPE	3. DATES COVERED (From - To)
August 2021	Technical Report	1 June 2019–30 April 2021

4. TITLE AND SUBTITLE
Investigation of Thermoelastic Damping in Microelectromechanical System (MEMS) Quadruple-Mass Gyroscope (QMG) Designs

5a. CONTRACT NUMBER

5b. GRANT NUMBER

5c. PROGRAM ELEMENT NUMBER

6. AUTHOR(S)
Alex Mazzoni, Ryan Rudy, Ryan Knight, and Jeff Pulskamp

5d. PROJECT NUMBER

5e. TASK NUMBER

5f. WORK UNIT NUMBER

7. PERFORMING ORGANIZATION NAME(S) AND ADDRESS(ES)
DEVCOM Army Research Laboratory
ATTN: FCDD-RLS-SA
2800 Powder Mill Rd
Adelphi, MD 20783

8. PERFORMING ORGANIZATION REPORT NUMBER
ARL-TR-9216

9. SPONSORING/MONITORING AGENCY NAME(S) AND ADDRESS(ES)

10. SPONSOR/MONITOR'S ACRONYM(S)

11. SPONSOR/MONITOR'S REPORT NUMBER(S)

12. DISTRIBUTION/AVAILABILITY STATEMENT
Approved for public release: distribution unlimited.

13. SUPPLEMENTARY NOTES
ORCID ID: Alex Mazzoni, 0000-0002-8184-4373

14. ABSTRACT
Thermoelastic damping (TED) is an intrinsic damping source in microelectromechanical system resonators that limits the quality factor (Q). In this report, we document the process developed to model TED in quadruple-mass gyroscope (QMG) designs using COMSOL Multiphysics software. Modeled QMG TED performance is compared with experimental results and analytical models. Areas with low Q are found in the QMG designs where the anchor springs connect to the shuttles and potential design improvements are explored. The TED modeling process is then applied to a disk resonator gyroscope design and future experiments/modeling for device optimization are discussed.

15. SUBJECT TERMS
thermoelastic damping, quadruple-mass gyroscope, COMSOL, finite element analysis, MEMS resonator

16. SECURITY CLASSIFICATION OF:			17. LIMITATION OF ABSTRACT	18. NUMBER OF PAGES	19a. NAME OF RESPONSIBLE PERSON
a. REPORT	b. ABSTRACT	c. THIS PAGE			Ryan Rudy
Unclassified	Unclassified	Unclassified	UU	56	19b. TELEPHONE NUMBER (Include area code) (301) 394-2324

Standard Form 298 (Rev. 8/98)
Prescribed by ANSI Std. Z39.18

Contents

List of Figures

List of Tables

1. Introduction and Motivation

The military is reliant upon a signal from global positioning system (GPS) satellites for a multitude of position, navigation, and timing (PNT) purposes. This reliance on a GPS signal presents a limitation and potential liability as satellite signals are easily blocked by physical phenomena and are vulnerable to electromagnetic jamming. For this reason, the US Army Combat Capabilities Development Command Army Research Laboratory is interested in achieving accurate PNT in GPS-restricted environments. Of the various ways to achieve autonomous or local PNT systems, this report focuses on improving the performance of silicon-based microelectromechanical system (MEMS) resonators—specifically the quadruple-mass gyroscope (QMG).

1.1 Overview of MEMS-Based Quadruple-Mass Gyroscopes

The QMG, a type of Coriolis vibratory gyroscope (CVG), is a complex spring-mass system with orthogonal vibrational modes of operation. To understand how the QMG detects rotation, it is easier to demonstrate a simpler structure's operation. In a spring-mass system with a single mass and two orthogonal modes of vibration (Fig. 1), one vibrational axis serves as the drive axis and the other as the sense axis. The drive axis vibrational mode is externally driven and rotation of the device, **Ω**, causes vibration in the orthogonal direction (along the sense axis) due to the Coriolis force. The vibration along the sense axis can be used to calculate the rotation rate of the device.

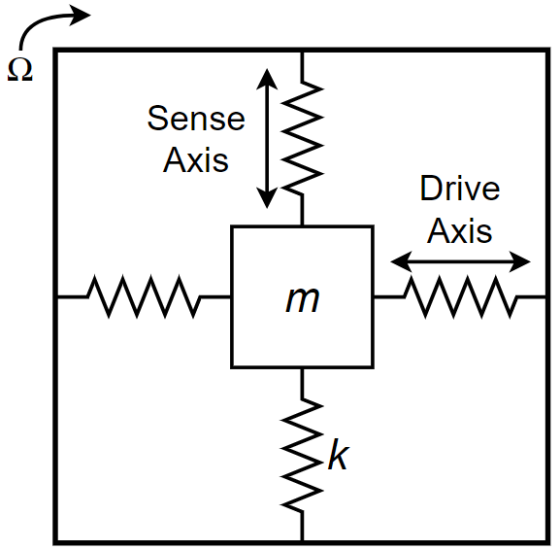

Fig. 1 Overview of a single-mass CVG; mass denoted by *m*, springs by *k*, and rotation by Ω

In a QMG the same principles of detecting rotation exist, but the spring-mass structure is more complex (Fig. 2). Four masses are driven along a particular vibrational direction and are forced to be vibrating in an anti-phase motion due to a connecting beam on the periphery of every adjacent mass. The masses are driven either electrostatically or piezoelectrically and the Coriolis force due to any rotation is detected along the sense-axis capacitively or piezoelectrically.

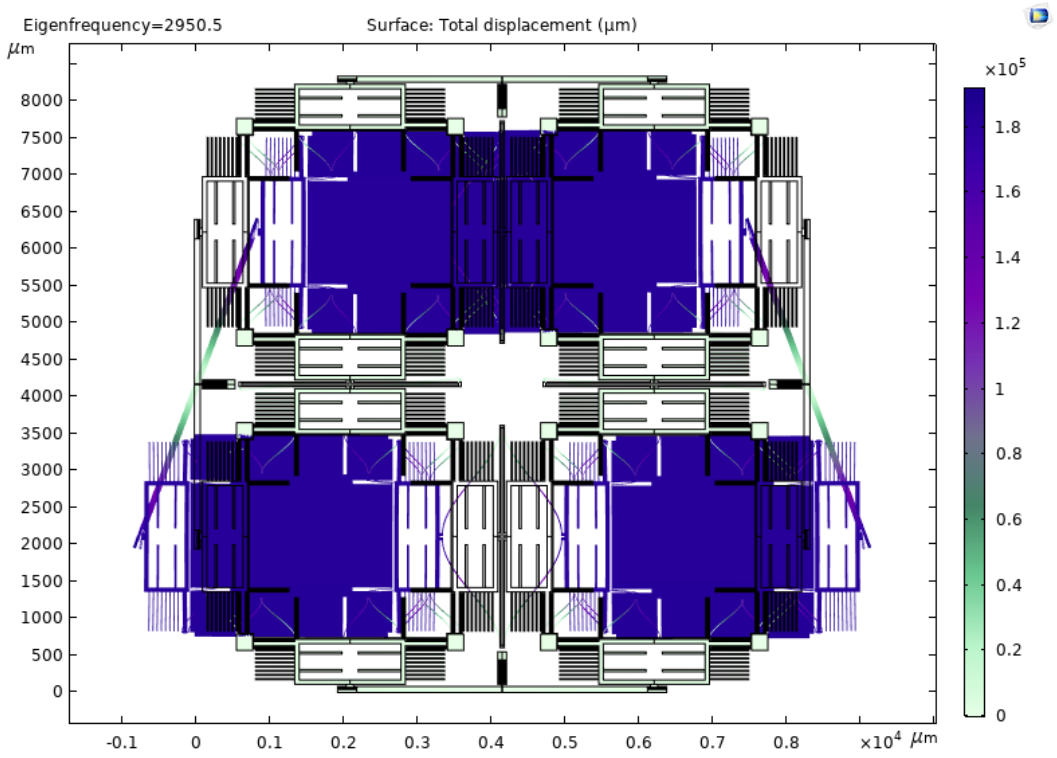

Fig. 2 COMSOL mode shape results of a QMG operating in the correct anti-phase mode

To quantify the performance of vibratory gyroscopes like the QMG, there are commonly used metrics such as bias stability, scale factor, and angle random walk (ARW). Leland derived expressions for the mechanical contribution to ARW of MEMS gyroscopes in both the open-loop and force-to-rebalance mode of operation.[1]

Open-loop:

$$\mathrm{ARW_{MTN}} \approx \sqrt{\frac{k_B T \omega_y}{A^2 M \omega_x^2 Q_y}\left[1+\left(\frac{Q_y\left(\omega_y^2-\omega_x^2\right)}{\omega_x \omega_y}\right)^2\right]^{-1}}\ \frac{rad}{\sqrt{sec}}$$

Closed-loop (force-to-rebalance mode):

$$\mathrm{ARW_{MTN}} \approx \sqrt{\frac{k_B T \omega_y}{A^2 M \omega_x^2 Q_y}\left[1+\left(\frac{Q_y(\omega_y^2-\omega_x^2)}{\omega_x \omega_y}\right)^2\right]}\frac{rad}{\sqrt{sec}})$$

where k_B is Boltzmann's constant, T is temperature, ω_x and ω_y are the resonant frequencies along the corresponding axes, A is drive axis displacement, M is the mass, and Q is the quality factor.

It is clear from the metrics that frequency-mismatch and Q are the dominating terms that impact device performance. In this report, we will focus mainly on the quality factor. Front-end signal buffering electronics also electrically contributes to ARW and this source is beyond the scope of this technical report.

1.2 Quality Factor and Damping Mechanisms in Vibratory MEMS-Based Quadruple-Mass Gyroscopes

As a MEMS resonator vibrates, potential energy is repeatedly stored in different areas of the device through the conversion of potential energy to kinetic energy and vice versa. The quality factor, Q, represents the efficiency with which the system exchanges stored energy. If the system had perfect efficiency or zero damping it would have an infinite Q and the spring-mass system would resonate forever. An analytical expression for Q is as follows in terms of energy stored and energy dissipated:

$$Q = 2\pi \frac{Energy\ Stored\ in\ System}{Energy\ Lost\ per\ Cycle}$$

1.2.1 Thermoelastic Damping

Materials like silicon that possess a positive coefficient of thermal expansion (CTE) cool down under tension and heat up during compression. A MEMS resonator like the QMG has components that cyclically expand and contract, therefore cyclically changing temperature as well. Thermal gradients across flexing parts of the resonator cause heat flow. This heat flow, generating entropy, is an irreversible loss of energy that can limit the quality factor, called thermoelastic damping (TED).

A commonly used analytical approximation to describe a quality factor due to TED, Q_{TED}, in a beam was derived by Zener.[2] An exact solution to the beam investigated by Zener has been calculated,[3] as well as solutions for more complex and realistic scenarios such as 2-D heat conduction.[4] However, especially at lower frequencies, the Zener model can be used as an accurate starting point for analysis:

$$Q_{TED} = \left[\frac{\rho C_{Si}}{E\alpha^2 T_0}\right]\frac{1 + (\omega\tau)^2}{\omega\tau},\ \tau = \left[\frac{W}{\pi}\right]^2 \frac{\rho C_{Si}}{\kappa},\ \omega = 2\pi f$$

where ρ is material density, C_{Si} is specific heat capacity, E is Young's modulus, α is CTE, T_0 is temperature, κ is thermal conductivity, W is beam width, and ω is angular frequency. τ represents the time constant of the thermal mode.

When the mechanical mode is significantly slower than the thermal mode (isothermal), the beam is approximately in a thermal equilibrium and minimal energy is dissipated. Similarly, when the mechanical mode is significantly faster than the thermal mode (adiabatic), there is not enough time for thermal relaxation and minimal energy is dissipated.[3] When the mechanical resonance frequency matches the thermal frequency, TED is at its maximum (Debye peak). At the Debye peak, Q_{TED} is determined solely by the intrinsic material properties, and thus material properties determine the absolute minimum Q_{TED} regardless of geometry. Figure 3 shows the result of using Zener's model with a 10 µm beam and the silicon material properties listed in Table 1.

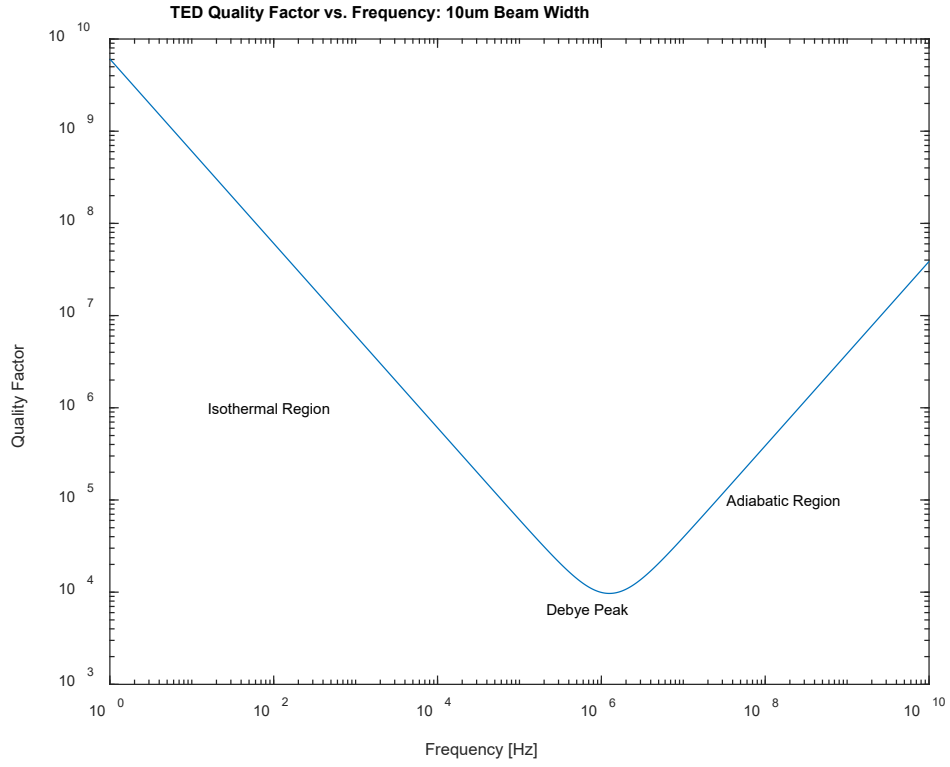

Fig. 3 Zener beam model applied to a 10 µm wide silicon beam

Table 1 Material parameters of silicon

Variable	Value	Units	Physical definition
ρ	2330	kg/m^3	Density
α	2.6*10^{-6}	K^{-1}	Coefficient of thermal expansion
C_{si}	700	J/(kg·K)	Specific heat capacity
κ	130	W/(m·K)	Thermal conductivity
E	170	GPa	Young's modulus

Notes: Values listed are from COMSOL's material library for single-crystal silicon.

1.2.2 Other Damping Mechanisms

Damping mechanisms other than TED can also limit the quality factor in vibratory MEMS devices. A concise overview of these damping mechanisms can be found in the paper by Rodriguez et al.[5] Assuming an independence between damping mechanisms, an overall quality factor can be calculated by reciprocally adding the Q limited by each damping mechanism:

$$\frac{1}{Q_{TOTAL}} = \frac{1}{Q_{viscous}} + \frac{1}{Q_{surface}} + \frac{1}{Q_{TED}} + \frac{1}{Q_{anchor}} + \frac{1}{Q_{Akhiezer}}$$

Previous work at DEVCOM Army Research Laboratory has improved the Q due to viscous damping by vacuum-packaging the QMG in the sub-μtorr regime.[6] Improvements in the tuning of resonators has also led to significant reduction in damping from anchor loss by matching the stiffness of the anti-phase motion.[7] With the improvements to address viscous and anchor loss damping, the role of TED has become more important. This report focuses on efforts to increase Q_{TED} in our QMG designs.

1.3 Experimental Goals

The experimental goals for this study were as follows:

- Develop a method to model TED for entire QMG designs
- Develop analytical TED models to inform design decisions and trade-offs
- Compare modeled TED performance of different QMG designs
- Determine potential areas of improvements in QMG designs
- Compare modeled TED performance to experimental measurements and simple analytical models
- Apply TED model to other designs → disk resonator gyroscope (DRG)

2. Methods

To achieve the goals listed in Section 1.3, the primary work done was the simulation of thermoelastic damping in various designs using the finite element analysis software COMSOL. Analytical models were scripted and visualized in MATLAB (2019A).[8]

This section covers details of how the COMSOL simulations were setup, including information such as boundary conditions, meshing, material parameters, COMSOL functions called, and notation utilized to interpret the results.

2.1 COMSOL Simulation Setups

The basis for all the TED simulations is the model provided by COMSOL in their MEMS Module titled "Thermoelastic Damping in a MEMS Resonator".[9] This model provides instruction for how to correctly set up the multiphysics link between Solid Mechanics and Heat Transfer in Solids, as well as the solver configuration to get a quality factor due to only TED. COMSOL version 5.5 was used, and simulations were run on a desktop PC with 32 GB of random access memory (RAM) and dual Intel Xeon E5-2620 v3 processors.

2.1.1 COMSOL 3-D Beam Tutorial Template

The basic 3-D model provided by COMSOL simulates a fixed-fixed beam that is 400 µm × 12 µm × 12 µm in size. Every simulation requires the establishment of two boundary conditions:

1) An anchor point, where the physical displacement will be set to zero
2) A temperature setpoint, where that boundary will be set to a reference temperature.

Often these conditions are set up at the same location in the simulation. In this model, the two ends of the beam highlighted in blue act as the "zero displacement" and "constant temperature" condition (Fig. 4).

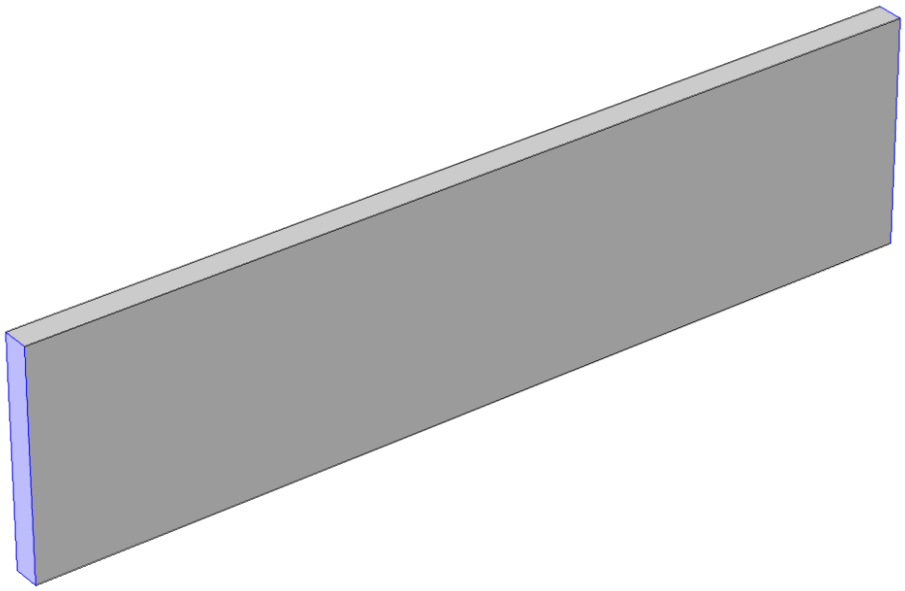

Fig. 4 Basic layout of the 3-D thermoelastic damping model provided in COMSOL's MEMS package, changed to 100 µm thick to represent the QMG thickness

2.1.2 Spring-Mass-Spring TED Simulations

It is computationally cumbersome to simulate an entire QMG, especially in 3-D or with a fine 2-D mesh. To gather information about simulation accuracy and computation time, simple 2-D and 3-D spring-mass-spring templates were developed.

A 2-D, two-spring simulation (Fig. 5) was created to test individual representative springs in an isolated manner and enable studies on mesh refinement and spring modification. To ensure the spring-mass system operates in the correct manner, two symmetry lines (green in Fig. 5) are established. These lines have the boundary condition that there can be no displacement through them, meaning in this case the mass should move purely in the y-direction or up and down.

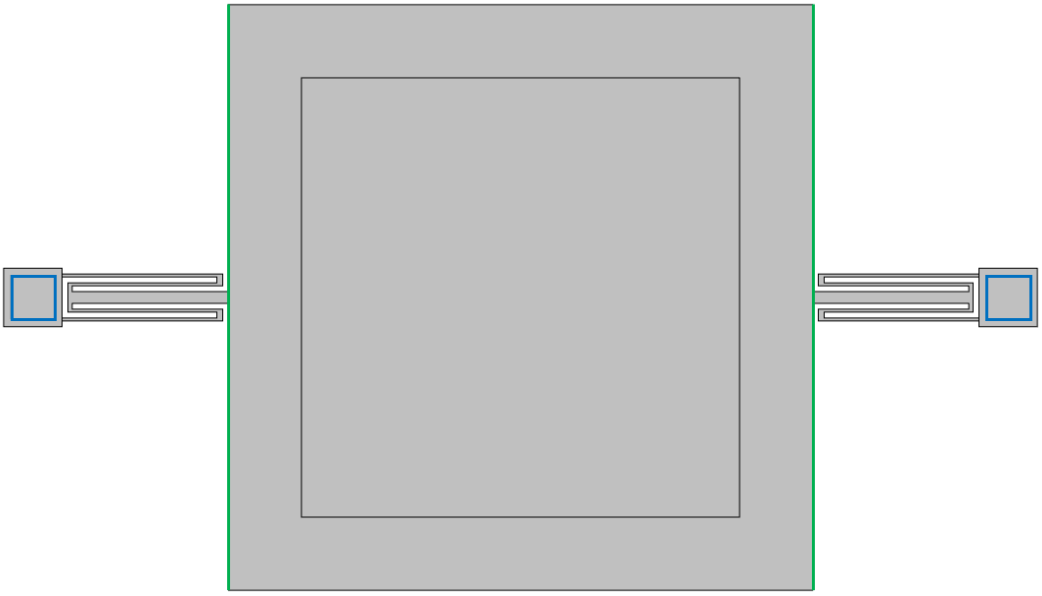

Fig. 5 Spring-mass-spring template used to simulate performance of individual springs. The blue squares are the anchor points, and the green lines are established symmetry conditions.

The blue squares on both sides are the anchor points where there is no displacement and there is constant temperature. The anchor is offset 25 μm from the edges to better represent the undercut at anchor points after performing the hydrofluoric acid vapor release etch. The inner square in the mass is there to allow the COMSOL user to change the frequency of operation by changing the center square's density. By keeping this variable-density area away from the springs, impact on the TED modeling is negligible.

To compare 2-D and 3-D simulations without using symmetry conditions and sacrificing mesh quality, a four-spring layout was created (Fig. 6).

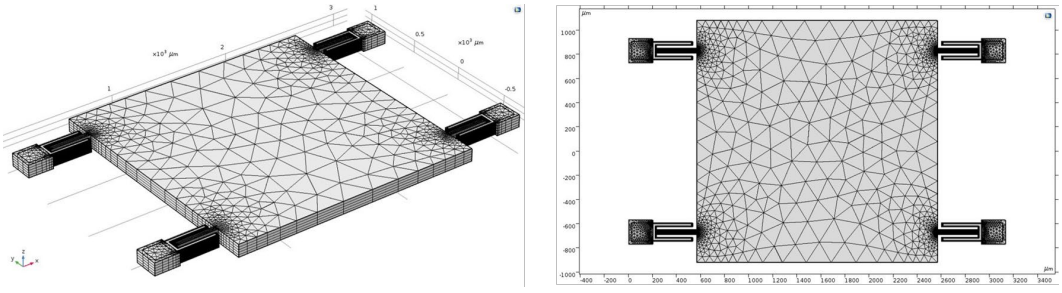

Fig. 6 Layout created to compare spring performance in 3-D (left) vs. 2-D (right) designs

2.1.3 2-D Whole-QMG TED Template

Figure 7 shows an example QMG computer-aided design (CAD) imported into COMSOL.

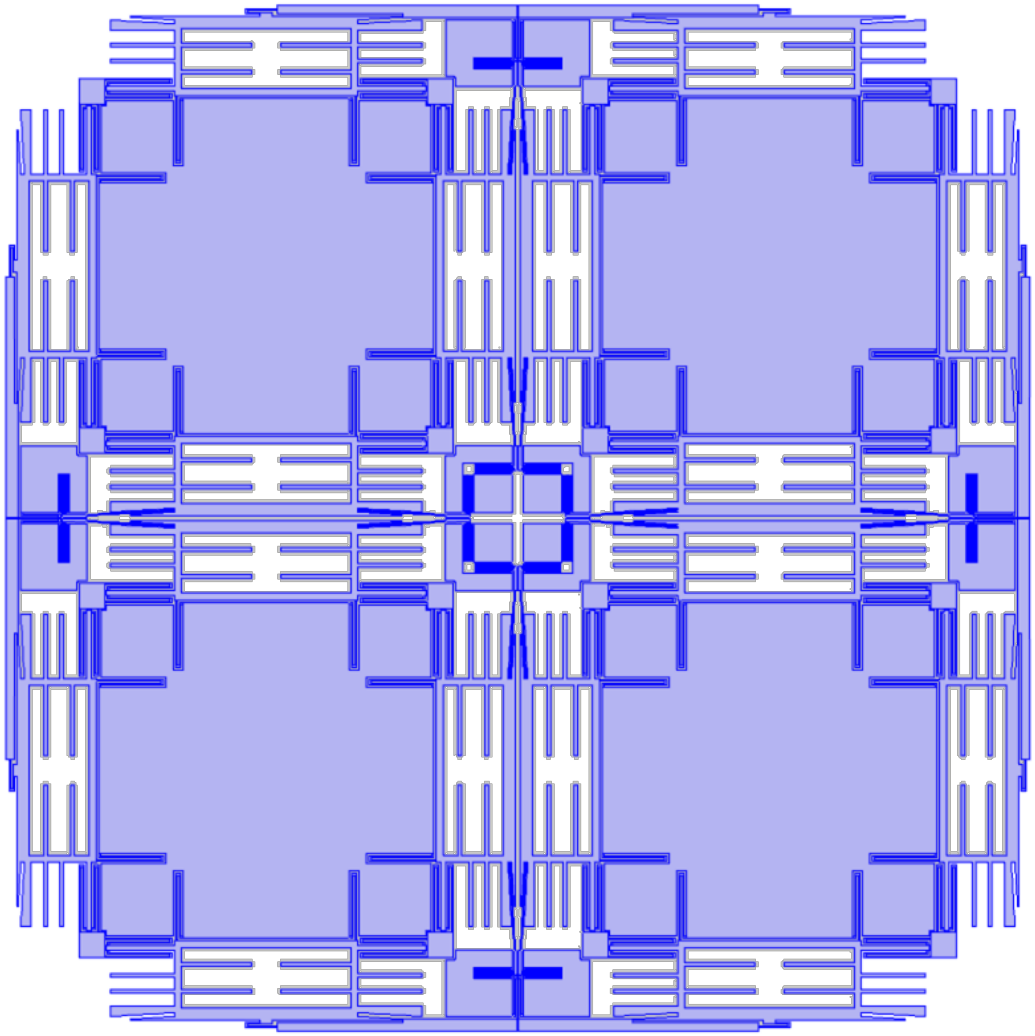

Fig. 7 QMG CAD after importing into COMSOL and selecting areas active domains (blue)

Areas shaded in blue are silicon and normally much of the interior white space would be filled with comb fingers to sense capacitance or drive motion, but they were removed to simplify the necessary meshing complexity. To demonstrate where the anchor points are chosen on a whole-QMG design, a quarter of the design is shown in Fig. 8 and the other quadrants are symmetric to this.

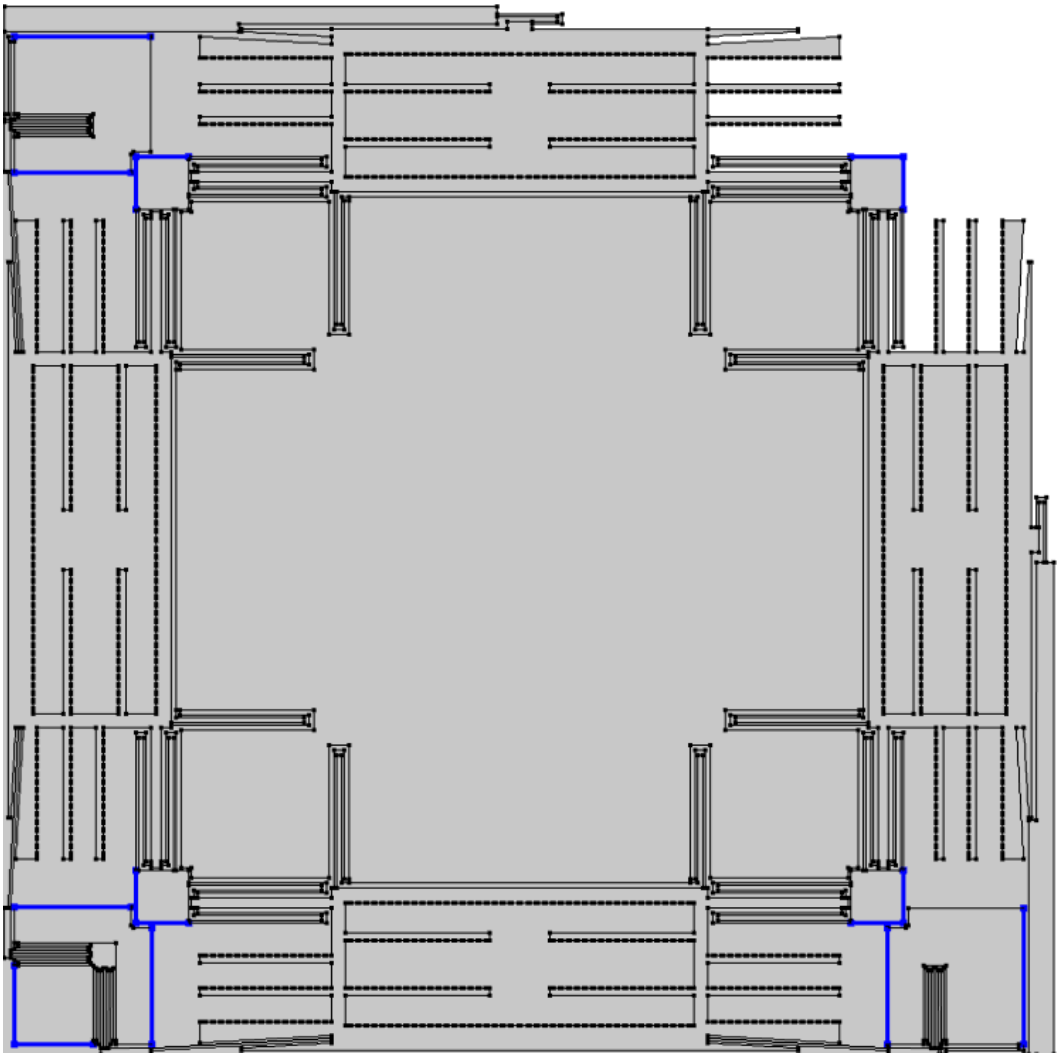

Fig. 8 Locations chosen in QMG designs for boundary conditions of both displacement and temperature

2.2 QMG Spring Notation

In our QMG designs, the four masses are interconnected by six different types of springs. Figure 9 shows a zoomed-in area of the top right of a QMG design to illustrate the six different springs. Figures 10–15 depict the distribution of each spring across an entire QMG design.

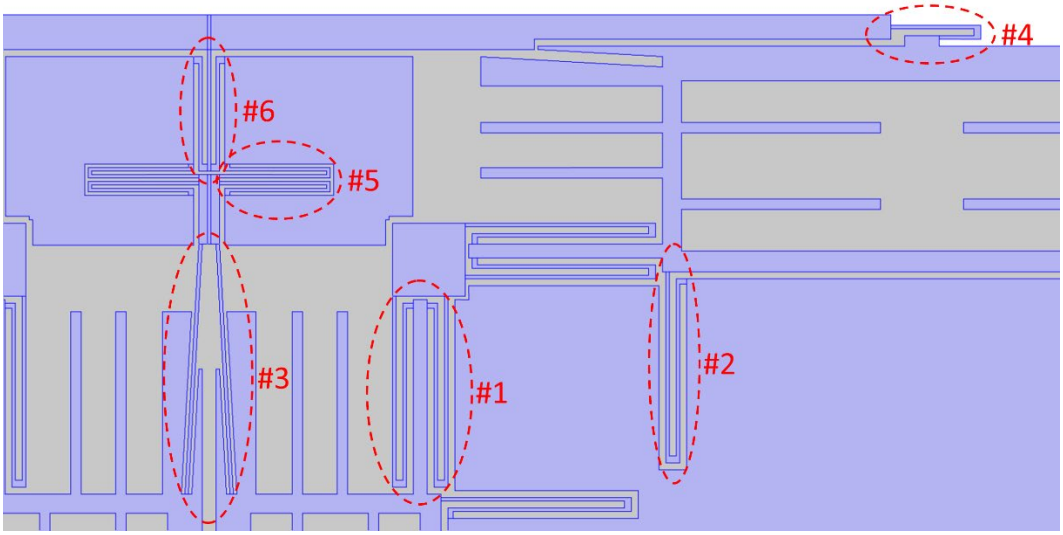

Fig. 9 Labeling utilized for springs in the QMG designs

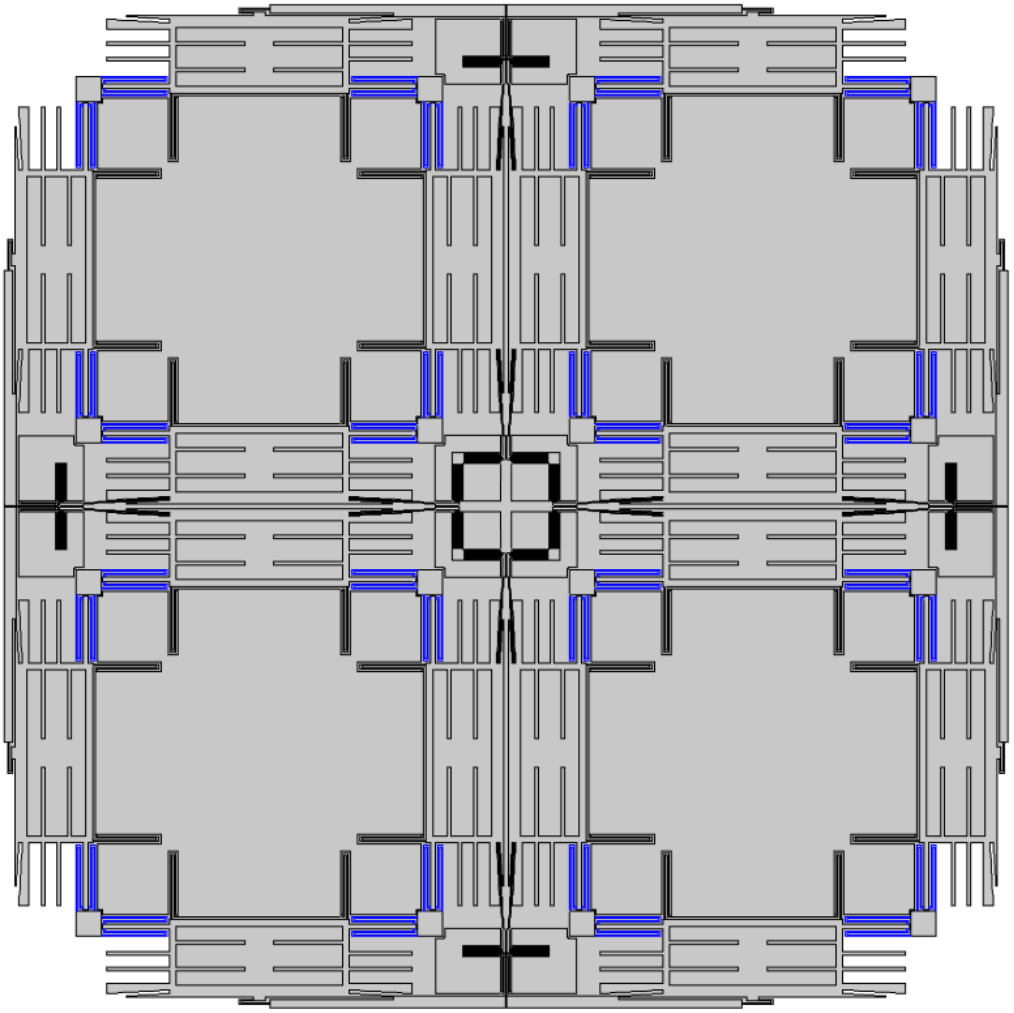

Fig. 10 Spring 1: anchor to proof mass and shuttle

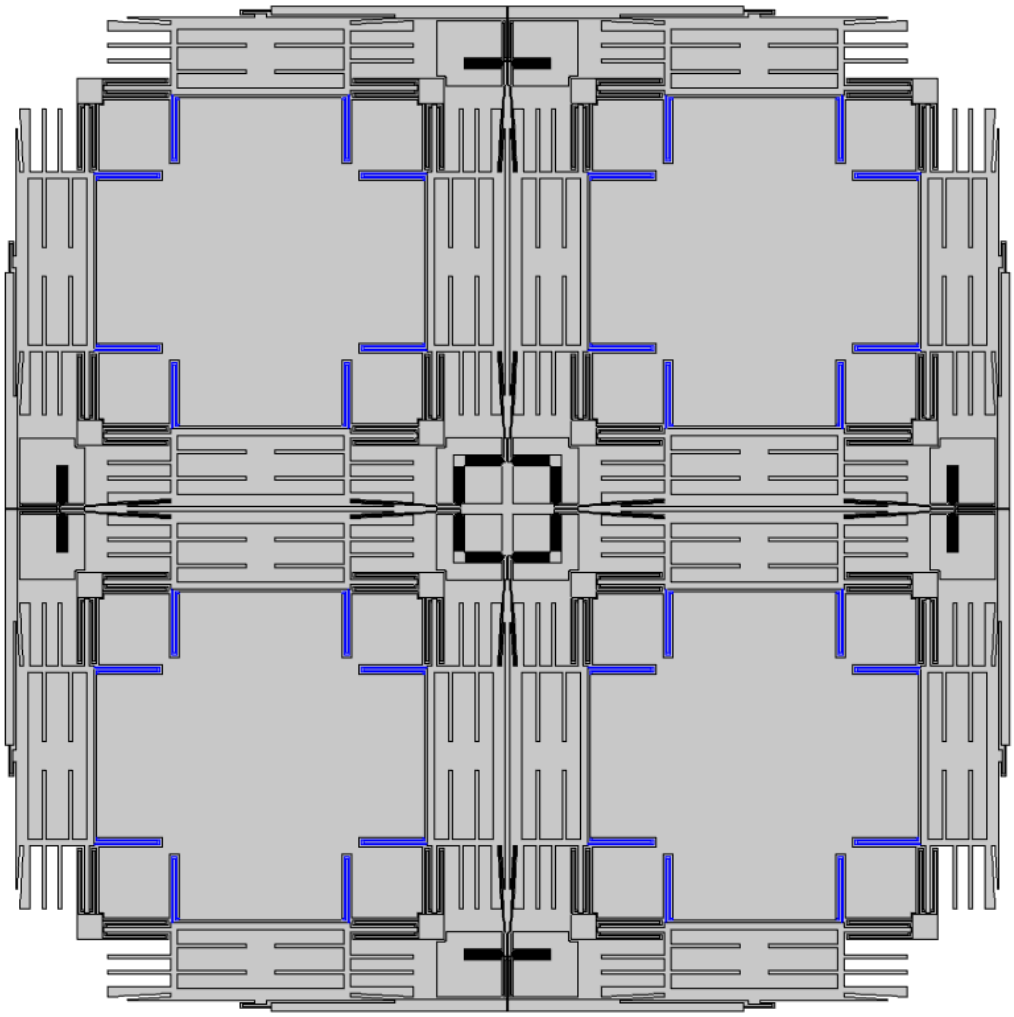

Fig. 11 Spring 2: proof mass to shuttle, constraining shuttle motion to a single direction

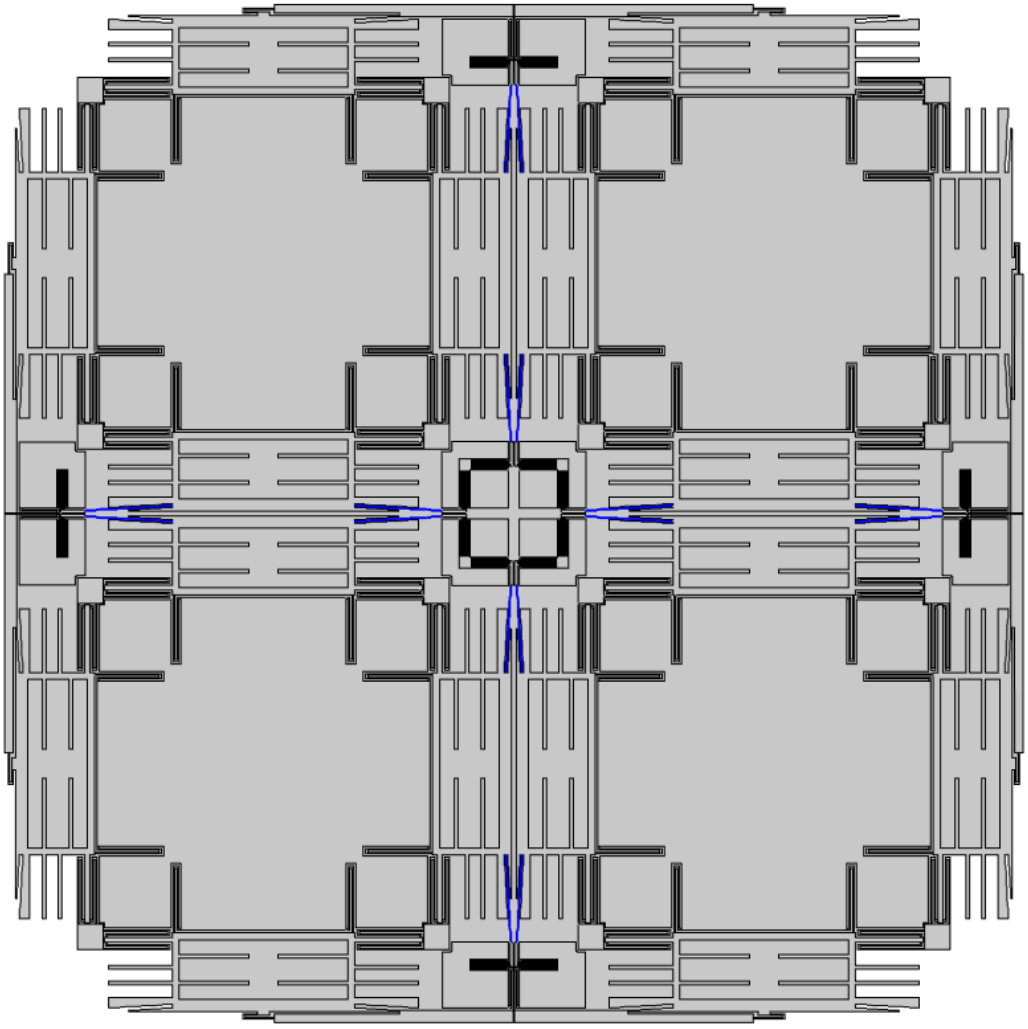

Fig. 12 Spring 3: shuttle to anchor coupling springs that create a preferential anti-phase mode

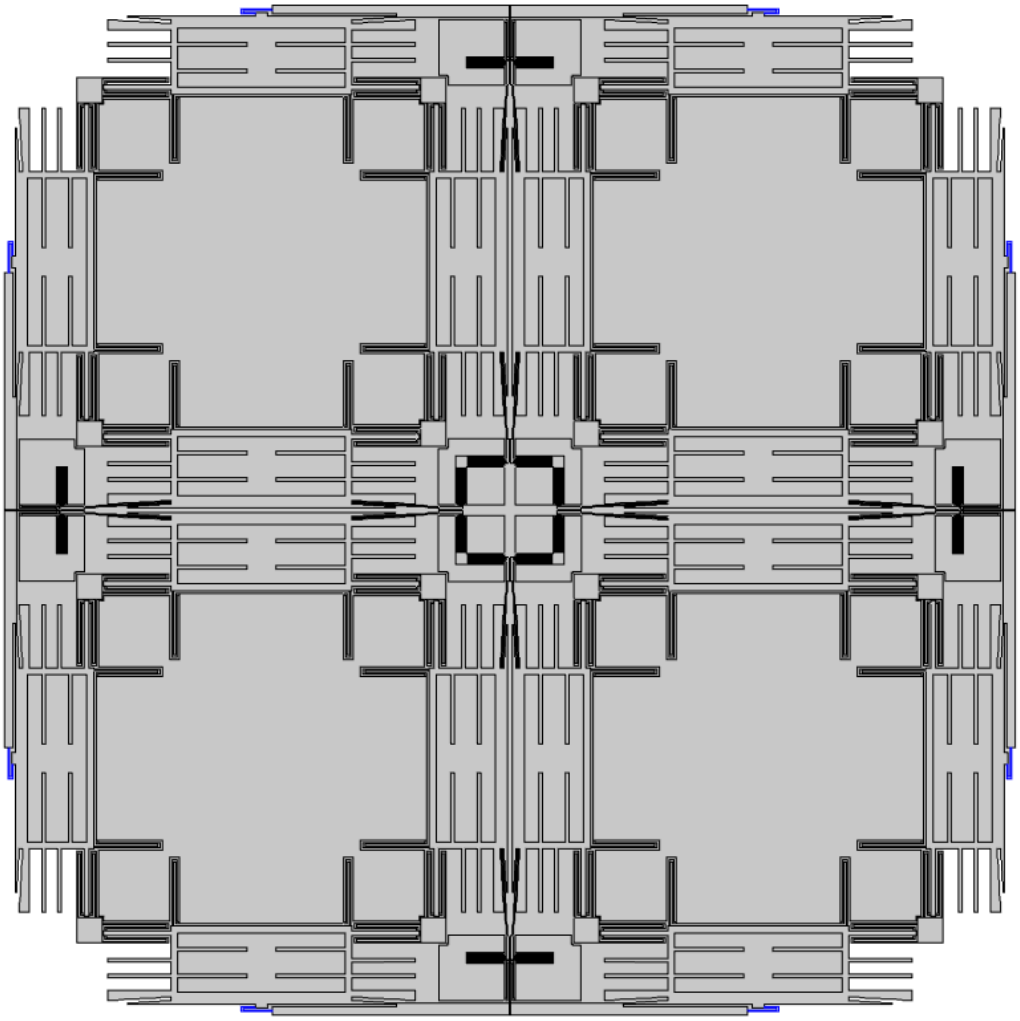

Fig. 13 Spring 4: shuttle to lever spring that allows rotation of the lever enforcing anti-phase motion

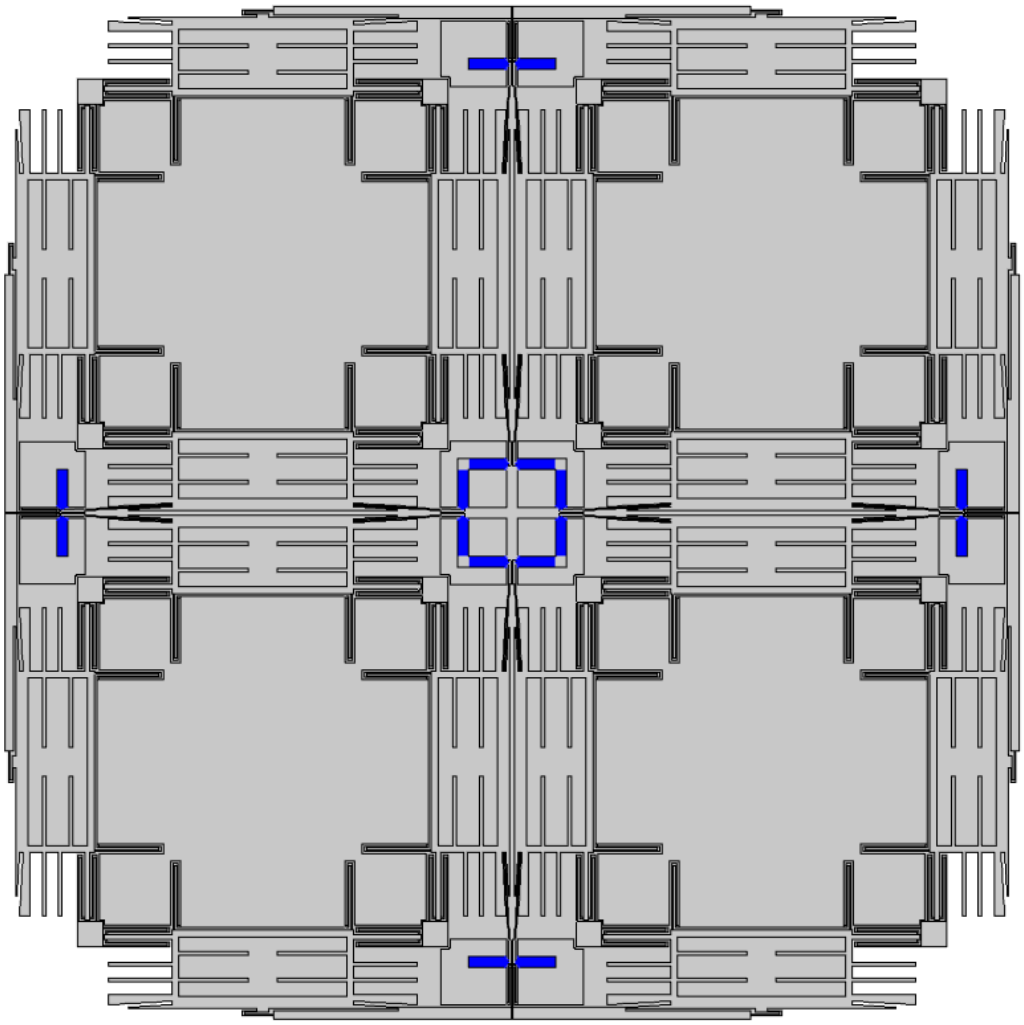

Fig. 14 Spring 5: coupling springs to anchor allowing for improved linearity

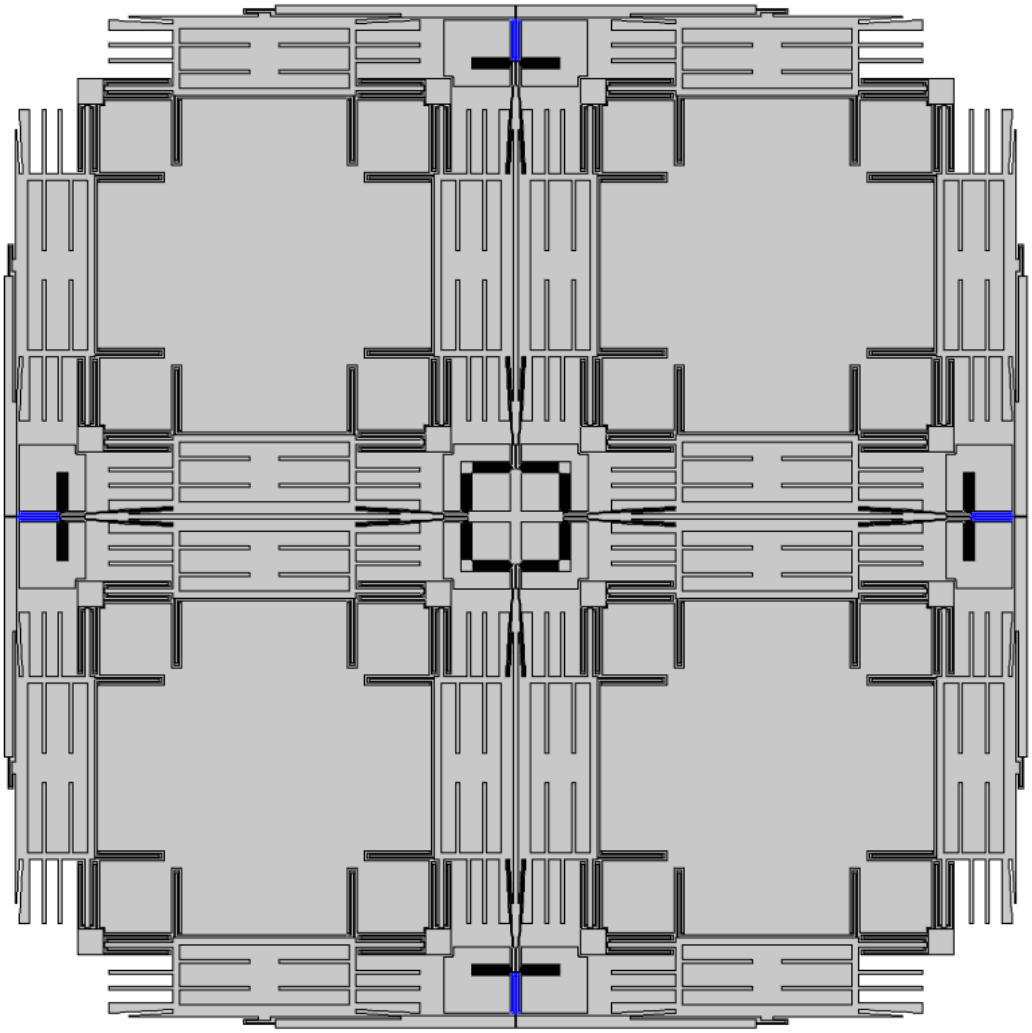

Fig. 15 Spring 6: lever to anchor allowing for rotation of lever

2.3 COMSOL Material Parameters and Functions

COMSOL has a built-in material called "Silicon (single crystal, anisotropic)" that comes preloaded with the full anisotropic elasticity matrix and values for density, thermal conductivity, heat capacity, and coefficient of thermal expansion. The values used for all simulations shown in this report were presented before in Table 1; however, the default elasticity matrix COMSOL provides incorrectly assumes the x-axis and y-axis of the design aligns with the [100] and [010] crystal directions.

To get correct elasticity matrix for a (100) or (111) wafer design[10,11] the following matrices need to be typed in with the option for Voigt notation selected (Fig. 16).

$$D_{100} = \begin{bmatrix} 194.4 & 35.2 & 63.9 & 0 & 0 & 0 \\ 35.2 & 194.4 & 63.9 & 0 & 0 & 0 \\ 63.9 & 63.9 & 165.7 & 0 & 0 & 0 \\ 0 & 0 & 0 & 79.6 & 0 & 0 \\ 0 & 0 & 0 & 0 & 79.6 & 0 \\ 0 & 0 & 0 & 0 & 0 & 50.9 \end{bmatrix} (GPa)$$

$$D_{111} = \begin{bmatrix} 194.4 & 54.33 & 44.77 & 0 & -13.53 & 0 \\ 54.33 & 194.4 & 44.77 & 0 & 13.53 & 0 \\ 44.77 & 44.77 & 203.97 & 0 & 0 & 0 \\ 0 & 0 & 0 & 60.47 & 0 & 13.53 \\ -13.53 & 13.53 & 0 & 0 & 60.47 & 0 \\ 0 & 0 & 0 & 13.53 & 0 & 70.03 \end{bmatrix} (GPa)$$

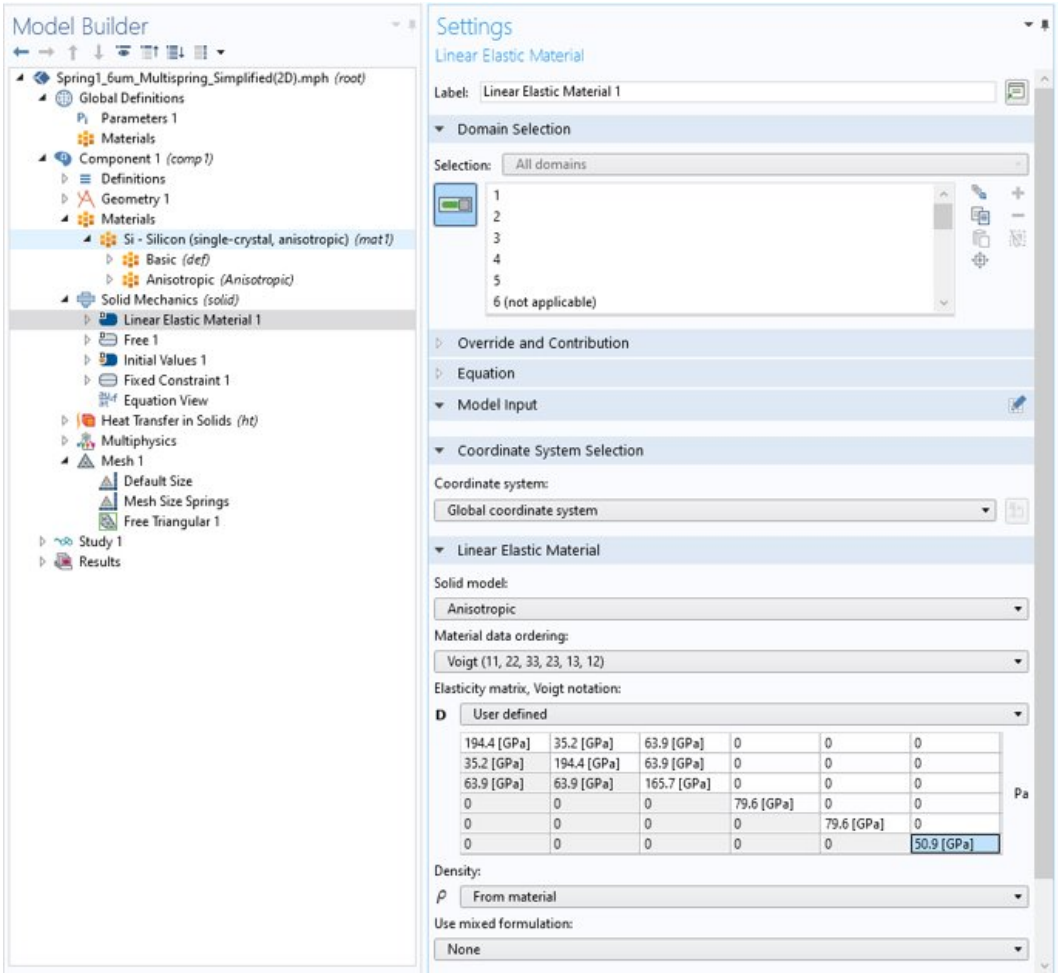

Fig. 16 How to change to the correct (100) elasticity matrix

COMSOL also has built-in functions to perform quick analysis of the coupled Solid Mechanics and Heat Transfer in Solids simulation results. Table 2 lists COMSOL functions employed to analyze the performance of individual spring components or overall QMG behavior.

Table 2 Useful COMSOL functions

Function name	Function units	Function description
solid.Ws	J/m^3	Elastic strain energy density
solid.Qted	W/m^3	Thermoelastic damping
solid.Q_eig	. . .	Quality factor for eigenvalue

The function solid.Ws returns the *cycle-average* of stored energy, defined as

$$W_s = \frac{1}{T}\int_0^T \frac{1}{2}\sigma(t):\varepsilon(t)\,dt = \frac{1}{4}real(\sigma:\overline{\varepsilon})$$

In Equation View, solid.Ws =

0.25*real(solid.el11*conj(solid.Sl11)+2*solid.el12*conj(solid.Sl12)+2*solid.el13*conj(solid.Sl13)+solid.el22*conj(solid.Sl22)+2*solid.el23*conj(solid.Sl23)+solid.el33*conj(solid.Sl33))

To get the *maximum stored energy*, *multiply solid.Ws by 2* (energy is function of x^2, x = sin(t))

Unique to and useful for TED modeling is the function solid.Qted, described in the MEMS Module User's Guide under "Theory of the Thermoelasticity Interface" section.[12]

The default expression for solid.Qted in COMSOL 5.5 is:

-linpoint(solid.T)*d(solid.Ent,TIME)

which is not a cycle-average of dissipated power and represents

$$Q_{TED1} = -T_1\left(\frac{\partial\varepsilon_0}{\partial T}\right)_\sigma : \frac{\partial\sigma_1}{\partial t}$$

The cycle average is $\langle Q_{TED1}\rangle = -\frac{1}{2}\mathrm{Re}\left\{T\left(\frac{\partial\varepsilon_0}{\partial T}\right)_\sigma : (i\omega\sigma)^*\right\}$

To make solid.Qted return the cycle average of power dissipation, go to "Equation View" under the "Thermal Expansion" Multiphysics. (Fig. 17) and change the expression to

solid.Qted = -0.5*real(lindev(T)*conj(lindev(solid.EntTIME)))*!isPML

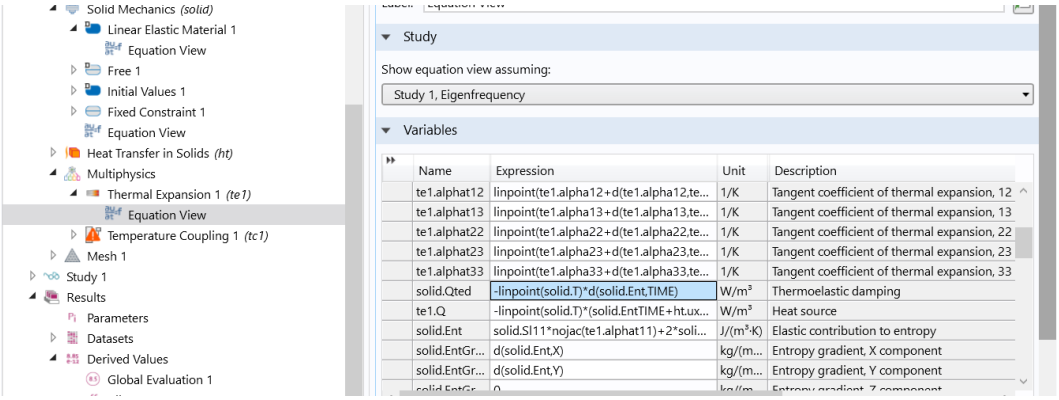

Fig. 17 Where to change expression for solid.Qted to the cycle average

By integrating solid.Ws and the updated solid.Qted, we can calculate a Q at a more localized, domain level—for instance a single spring in the QMG using this expression for quality factor:

$$Q = 2\pi f \frac{Energy\ Stored}{Power\ Loss}$$

Inserting solid.Ws for energy stored and solid.Qted for power loss,

$$Q_{TED,domain} = 4\pi f \frac{\int\int (solid.Ws)dA}{\int\int (solid.Qted)dA}$$

If $Q_{TED,domain}$ is calculated using every domain, then it returns the same value as the function solid.Q_eig, which returns the quality factor for the entire design based on the eigenvalue, λ, as

$$solid.Q\_eig = \frac{Imag(\lambda)}{2 \times Real(\lambda)}$$

3. Results

3.1 MATLAB TED Modeling

MATLAB was used to

- Provide design-space information about Freq, Q, T, beam width and include impact of α(T)
- Compare the TED performance of other materials

Figure 18 plots Q_{TED} versus frequency using Zener's model for silicon beam widths of 1–30 µm. The minimum Q_{TED} is independent of beam dimension and depends solely on temperature and the material properties α, C_{si}, ρ, and E. The frequency at

which that minimum occurs, however, is dependent on beam dimension, as well as C_{si}, ρ, and κ. The dashed line, Q_{AKE}, represents Akhiezer damping, another intrinsic source of damping caused by perturbations in the phonon distribution. Q_{AKE} represents the limit of possible device performance.[5]

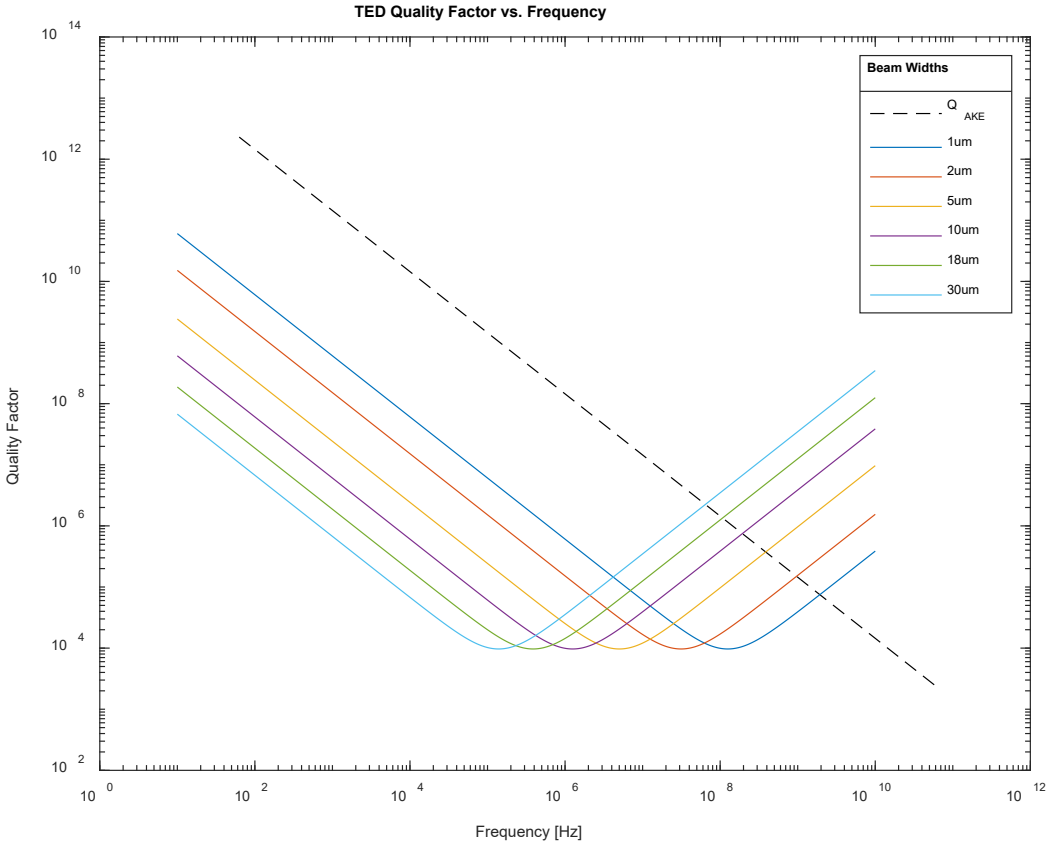

Fig. 18 Q_{TED} vs. frequency for silicon beam widths of 1–30 µm at 293 K

The width of the QMG springs is currently 10 µm, and it operates at less than 5 kHz. This places the QMG operation well into the isothermal regime. In this regime, $f \times Q_{TED}$ is constant for a given beam width. It is therefore useful to compare results using the $f \times Q_{TED}$ product.

Figure 19 contains a plot of Q at 2 kHz for a range of bean widths, *W,* highlighting that for beam widths smaller than 10 µm, Q_{TED} is inversely proportional to W^2.

$$Q_{TED} \propto \frac{1}{W^2}$$

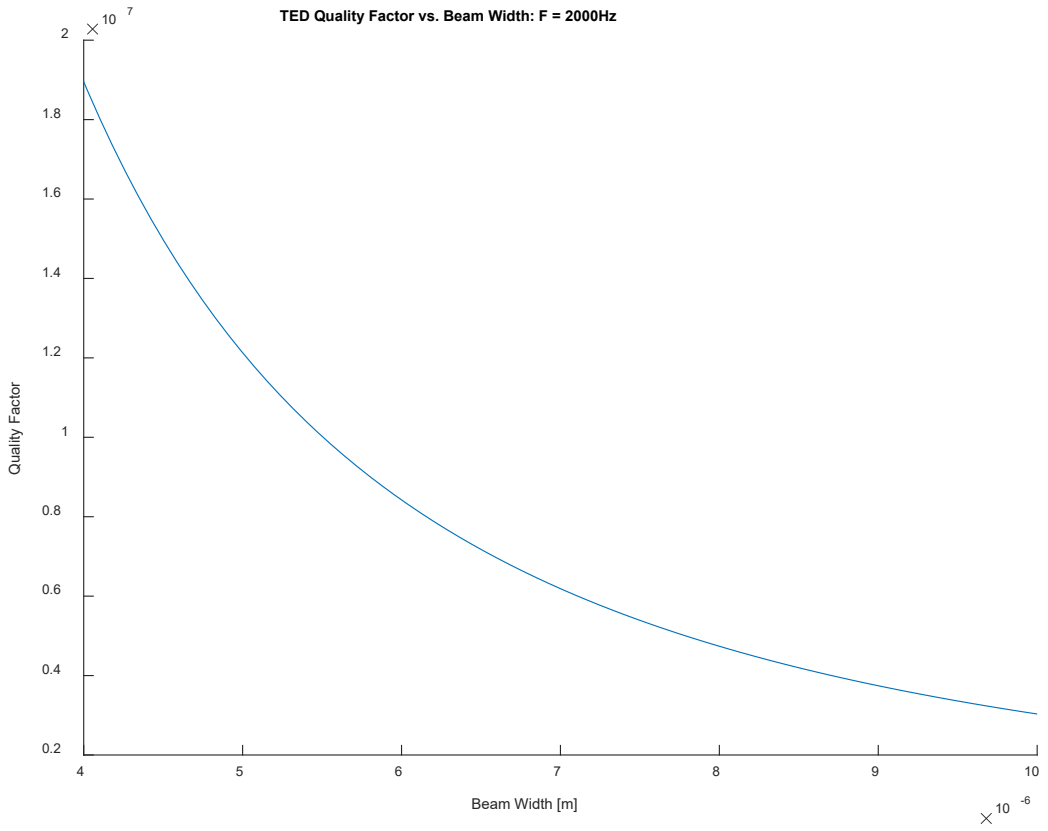

Fig. 19 Q_{TED} vs. beam width for an operation frequency of 2 kHz

We have been assuming a constant temperature; however, the CTE of silicon is a function of temperature, $\alpha_{si}(T)$ (Fig. 20).

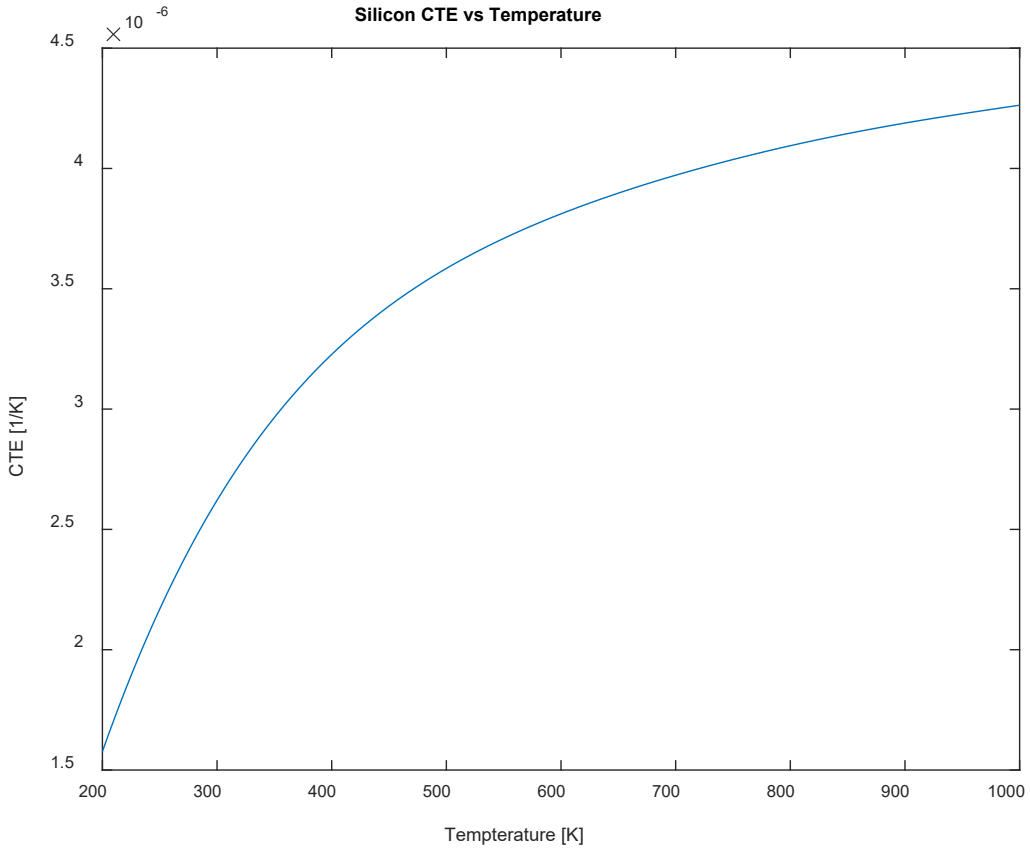

Fig. 20 $\alpha_{si}(T)$ as given by a fit of experimentally measured CTE values between 293 K to 1000 K.[13] We continued the function lower in temperature to 200 K to cover the military specification temperature range. The extracted lower temperature values for α_{si} compare well with low-temperature experimental measurements down to 200 K, but the model diverges upon further temperature decrease.[14]

By inserting $\alpha_{si}(T)$ into the Zener model, we can see how Q_{TED} changes over the military specification temperature range of −55 °C to 125 °C (~220 to 400 K, Fig. 21).

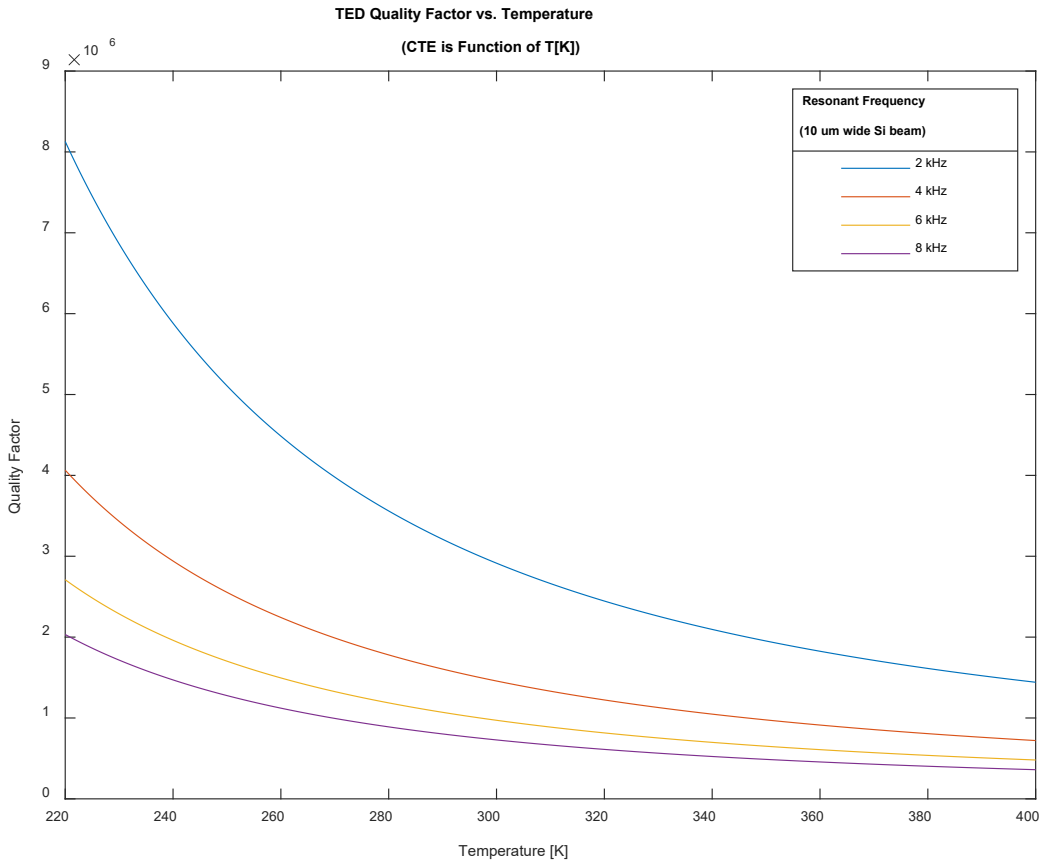

Fig. 21 Q_{TED} vs. temperature for a 10 µm wide silicon beam at various frequencies. Fitting this data to a power fit model ($y = Ax^n$), n = -2.8 at 300 K.

We can get the temperature coefficient of quality factor by taking $\frac{d(Q_{TED})}{dT}$ (Fig. 22) and normalizing the values with respect to Q_{TED} at 300 K (Fig. 23)

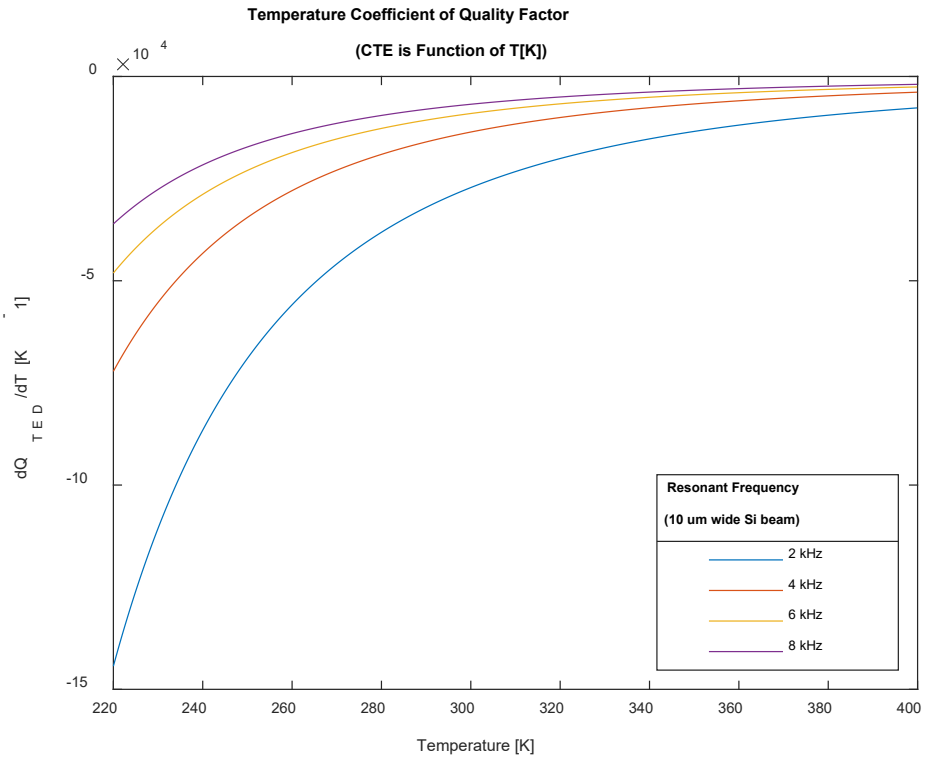

Fig. 22 Temperature coefficient of quality factor, not normalized

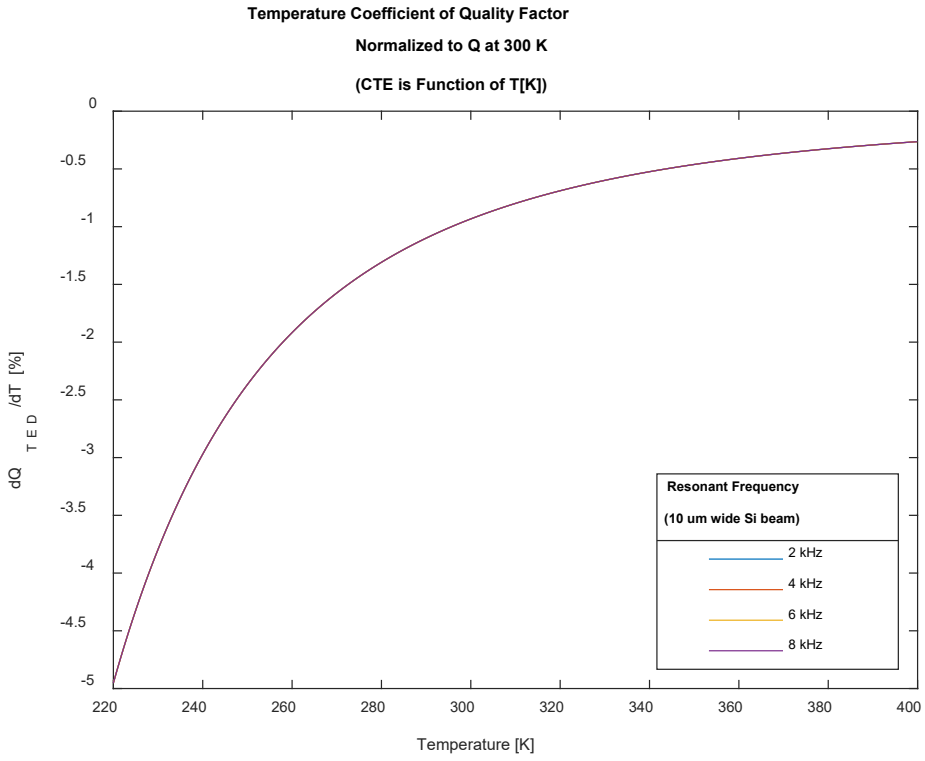

Fig. 23 Temperature coefficient of quality factor, normalized

Since Q_{TED} is an intrinsic source of damping at room temperature, a comparison of Q_{TED} performance between other potential materials is provided in Fig. 24, using the material properties in Table 3. In the relevant frequency ranges, the only materials performing better than silicon are diamond and Zerodur, a material specifically crafted for a low CTE.

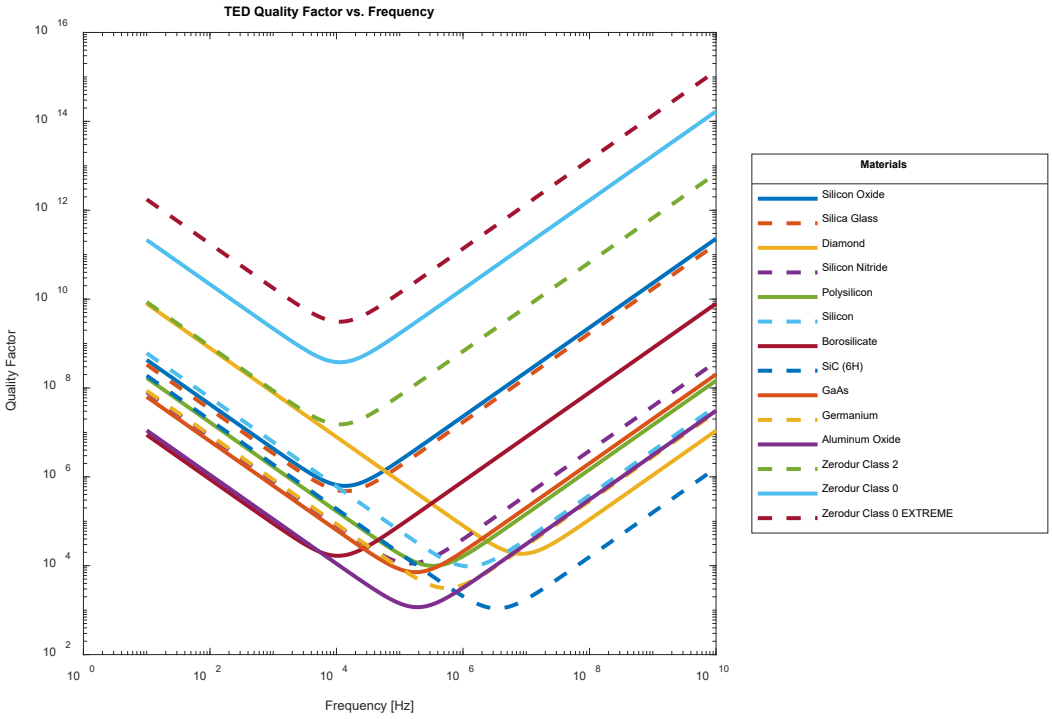

Fig. 24 Material comparison of Q_{TED} vs. frequency at 293 K

Table 3 Material properties used for Figure 24

Material	E (Pa)	CTE (1/K)	ρ (kg/m³)	Cp (J/(kg·K))	κ (W/(m·K))
Silicon oxide	7.00E+10	5.00E-07	2200	730	1.4
Silica glass	7.31E+10	5.50E-07	2203	703	1.38
Diamond	1.05E+12	8.00E-07	3515	520	990
Silicon nitride	2.50E+11	2.30E-06	3100	700	20
Polysilicon	1.60E+11	2.60E-06	2320	678	34
Silicon	1.70E+11	2.60E-06	2329	700	130
Borosilicate	6.30E+10	3.30E-06	2230	754	1.13
SiC (6H)	7.48E+11	4.30E-06	3216	690	490
GaAs	8.59E+10	5.70E-06	5316	550	33
Germanium	1.03E+11	5.90E-06	5323	310	58
Aluminum oxide	4.00E+11	6.50E-06	3965	730	35
Zerodur Class 2	9.10E+10	1.00E-07	2530	800	1.46
Zerodur Class 0	9.10E+10	2.00E-08	2530	800	1.46
Zerodur Class 0 EXTREME	9.10E+10	7.00E-09	2530	800	1.46

3.2 General TED Simulation Results

3.2.1 Impact of Beam Thickness and 2-D Approximation Choices

We used the tutorial fixed-fixed beam model to test the impact that beam height (equivalent to silicon thickness) has on frequency and Q, along with checking how the 2-D approximations compare to the 3-D simulations (Table 4).

Table 4 Fixed-fixed beam: impact of thickness and 2-D approximation

Thickness	Frequency	Q	F*Q	No. Z-mesh
12 µm	6.535E5+29.8i	10980	7.17E+09	5
25 µm	6.556E5+31.1i	10534	6.91E+09	5
50 µm	6.608E5+34.9i	9465.1	6.25E+09	5
100 µm	6.690E5+41.4i	8088.6	5.41E+09	5
100 µm	6.687E5+41.2i	8124.2	5.43E+09	10
100 µm	6.686E5+41.1i	8129.2	5.44E+09	15
200 µm	6.763E5+47.4i	7134.4	4.83E+09	5
400 µm	6.819E5+52.1i	6540.3	4.46E+09	5
2-D	6.870E5+56.8i	6046.2	4.15E+09	(Plane strain) 100 µm thickness
2-D	6.518E5+29.1i	11156	7.27E+09	(Plane stress) 100 µm thickness

Notes: Mapped and swept rectangular mesh with a distribution of 70 in the x-direction and 5 in the y-direction. 400 µm beam length, 12 µm beam width, varying beam thickness.

The QMG silicon thickness is 100 µm, falling between the two extremes of the plane strain and plane stress approximations. The plane strain approximation is used in this report because it gives closer results than the plane stress approximation and is computationally easier.

According to the fixed-fixed beam model for (100) silicon, to approximate the 100 µm 3-D performance based on the 2-D model, the frequency gets multiplied by a factor of 0.973 and Q by 1.345.

3.2.2 Mesh Refinement: Single Spring

There is a trade-off between simulating springs in a spring-mass-spring environment and a whole-QMG environment. In the spring-mass-spring environment one can push the mesh quality to finer levels to get a more accurate result of how that spring performs. However, in the spring-mass-spring setup the forces exerted on this spring and the motion it undergoes cannot accurately simulate what happens to this spring when put within the entire QMG design. A main assumption we make here is that by applying the symmetry boundary condition to ensure the mass moves in the correct direction we do not substantially change how

this spring operates. A test of the impact that the mesh quality of Spring 1 has on Q was performed, and the results are presented in Table 5.

Table 5 Single spring mesh refinement

Mesh definition	Domain elements	Boundary elements	Degrees of freedom	Simulation time	Freq (Hz)	Q
Max 5 µm	10966	2324	55120	9 s	2004.5	1.8609E+06
Max 4 µm	15360	2894	76308	10 s	2003.9	1.8554E+06
Max 2.5 µm	37606	4572	180580	24 s	2002.7	1.7820E+06
Max 2 µm	58808	5700	278789	32 s	2002.4	1.7696E+06
Max 1 µm	232150	11304	1072738	125 s	2001.6	1.7464E+06
Max 0.5 µm	902310	22512	4116278	623 s	2001.0	1.7418E+06

This result informs us of the potential error when performing whole-QMG simulations as we must choose a coarser mesh than a user-defined "Max 0.5 µm".

3.2.3 2-D vs. 3-D Simple Design

To understand the differences between running a 2-D and 3-D TED simulation on a more complex structure than a fixed-fixed beam, we compared 2-D and 3-D simulations of the four-spring and one-mass design described earlier (Fig. 6) using Spring 1 from a QMG design.

This comparison was made for both (100) silicon (Table 6) and for (111) silicon (Table 7).

Table 6 2-D vs. 3-D comparison for (100) silicon

Thickness (µm)	Spring mesh	Frequency (Hz)	Q	F*Q	No. of Z-meshes
100	Max 3.0	3574.7	2.8729E+06	1.03E+10	5
100	Max 2.0	3571.2	2.7381E+06	9.78E+09	5
250	Max 3.0	3626.6	2.3494E+06	8.52E+09	5
500	Max 3.0	3643.4	1.9964E+06	7.27E+09	5
2-D	Max 2.0	3649	1.99E+06	7.26E+09	N/A

According to this model for (100) silicon, to approximate the 100 µm 3-D performance based on a 2-D model, the frequency gets multiplied by approximately 0.98 and Q by approximately 1.35.

Table 7 2-D vs. 3-D comparison for (111) silicon

Thickness (µm)	Spring mesh	Frequency (Hz)	Q	F*Q	No. of Z-meshes
100	Max 2.0	3525.3	3.2755E+06	1.15E+10	5
2-D	Max 2.0	3583.4	2.4702E+06	8.85E+09	N/A

According to this model for (111) silicon, to approximate the 100 μm 3-D performance based on a 2-D model, the frequency gets multiplied by approximately 0.98 and Q by approximately 1.325.

3.3 Whole-QMG 2-D Simulations

3.3.1 QMG Mesh Refinement/Simulation Time

To start simulating entire QMG designs, we initially determined where the best trade-off was in terms of mesh density versus simulation time. Table 8 shows the results from trying different spring mesh sizes, while keeping all the other areas at the mesh size of "General Physics → Predefined → Extremely Coarse".

Table 8 2-D vs. 3-D comparison for (111) silicon

Mesh size	Time (s)	Domain elements	Boundary elements	Frequency (Hz)	Q
Extra fine semi.	142	185947	65894	3300.5	9.5459E+05
Extremely fine semi	358	510027	121634	3289.2	8.9253E+05
Maximum 2 μm	968	1166081	183112	3287.0	7.9601E+05
Maximum 1 μm	>18 h (out of RAM)	4309118	335345	. . .	. . .

This result led to the establishment of using a user-defined max 2.0 μm mesh on the springs of whole-QMG simulations to balance the accuracy and simulation time trade-off.

3.3.2 QMG Design Comparisons

Four different QMG designs were simulated for TED. Using the by-domain-Q analysis described earlier we were able to determine where in the QMG energy was being stored and dissipated. When adding up the energy stored and dissipated in the QMG springs compared to the overall amounts, a sign of underperformance was showing. The spring domains consistently accounted for approximately 97% of the energy storage, but only approximately 80% of the energy dissipation. It was determined that the shuttles (see Fig. 25) were responsible for storing a percent or two of the energy but dissipating 15% to 20%. Specifically, the anchor springs to shuttle connection point was where most dissipation was located (Fig. 26).

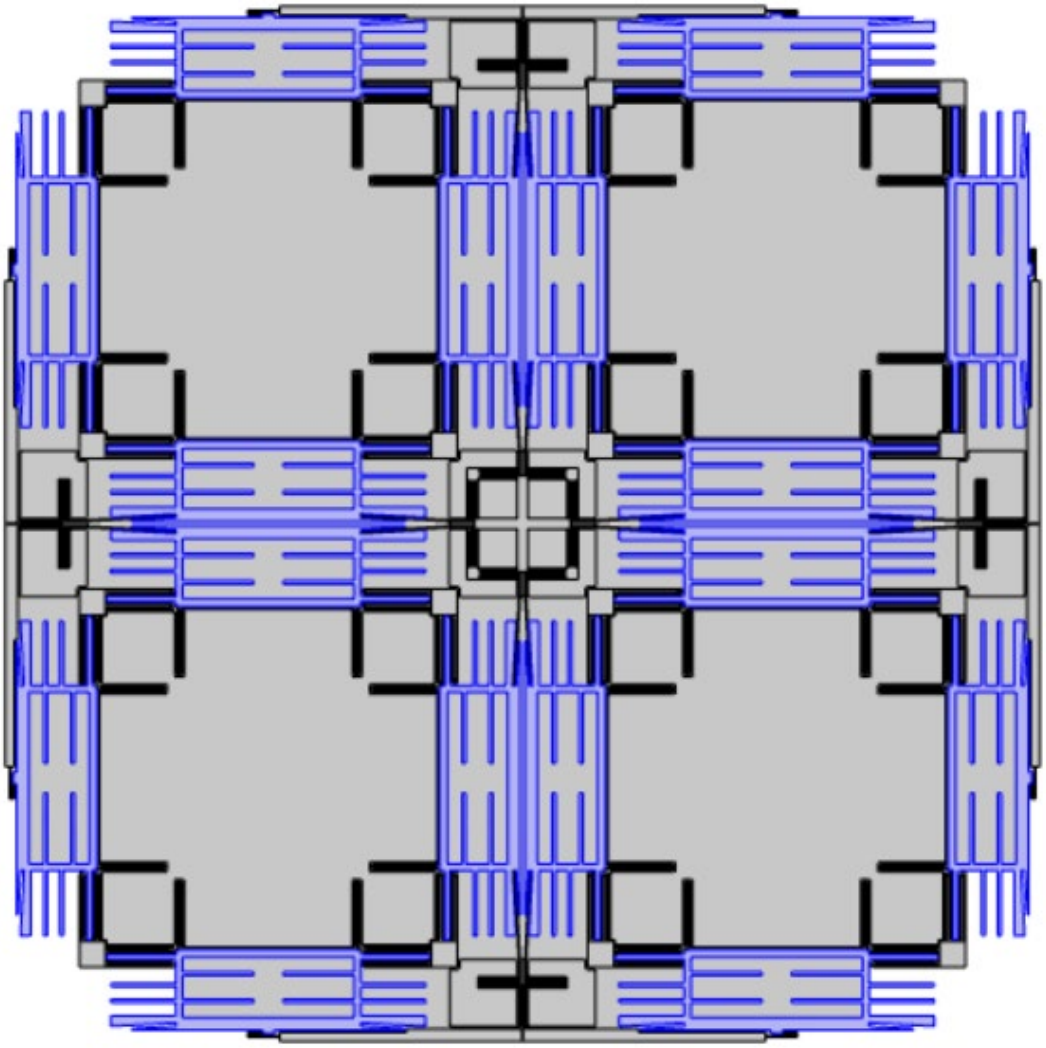

Fig. 25 Shuttles

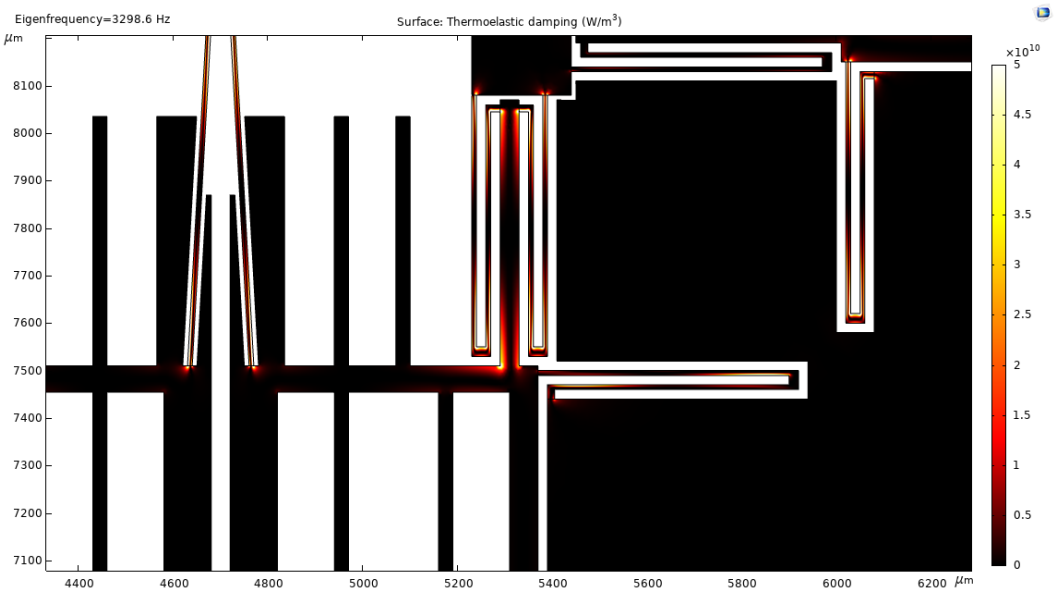

Fig. 26 Plot of solid.Qted that shows the low-Q_{TED} anchor spring to shuttle connection

Tables 9–12 show the performance of the four different QMG designs, with the inclusion of the shuttles as an area to study energy storage and dissipation.

Table 9 Q_{TED}-by-domain QMG Design 1

Design 1 (Old CAD)	Frequency (Hz)	Elastic energy (∭solid.Ws) (J/m)	TED (∭solid.Qted) (W/m)	Q due to TED	% Energy stored	% Energy dissipated
QMG	3298.9	1.27E+05	13316	7.905E+05	. . .	. . .
Spring 1	3298.9	70155	5817.6	9.998E+05	55.26	43.69
Spring 2	3298.9	38223	3365	9.418E+05	30.11	25.27
Spring 3	3298.9	13280	1044	1.055E+06	10.46	7.84
Spring 4	3298.9	134.72	12.014	9.297E+05	0.11	0.09
Spring 5	3298.9	505.5	39.659	1.057E+06	0.40	0.30
Spring 6	3298.9	315.96	27.553	9.508E+05	0.25	0.21
Shuttles	3298.9	2899.1	2577.6	9.325E+04	2.28	19.36
Total	. . .	. . .	. . .	. . .	**98.86**	**96.75**

Table 10 Q_{TED}-by-domain QMG Design 2

Design 2 (New CAD, 1 spring)	Frequency (Hz)	Elastic energy (∭solid.Ws) (J/m)	TED (∭solid.Qted) (W/m)	Q due to TED	% Energy stored	% Energy dissipated
QMG	3410.8	1.08E+05	12076	7.665E+05	. . .	. . .
Spring 1	3410.8	57144	5067.6	9.666E+05	52.92	41.96
Spring 2	3410.8	34792	3267.8	9.127E+05	32.22	27.06
Spring 3	3410.8	10837	916.81	1.013E+06	10.04	7.59
Spring 4	3410.8	327.25	27.094	1.035E+06	0.30	0.22
Spring 5	3410.8	753.8	66.153	9.768E+05	0.70	0.55
Spring 6	3410.8	305.14	27.953	9.358E+05	0.28	0.23
Shuttles	3410.8	2489.2	2214.4	9.636E+04	2.31	18.34
Total	. . .	. . .	. . .	. . .	**98.77**	**95.96**

Table 11 Q_{TED}-by-domain QMG Design 3

Design 3 (New CAD, 2 springs)	Frequency (Hz)	Elastic energy (∭solid.Ws) (J/m)	TED (∭solid.Qted) (W/m)	Q due to TED	% Energy stored	% Energy dissipated
QMG	3965.3	1.61E+05	24721	6.507E+05	. . .	. . .
Spring 1	3965.3	66517	8082.2	8.202E+05	41.21	32.69
Spring 2	3965.3	75115	9070.3	8.253E+05	46.54	36.69
Spring 3	3965.3	12541	1430.8	8.735E+05	7.77	5.79
Spring 4	3965.3	377.39	42.151	8.923E+05	0.23	0.17
Spring 5	3965.3	872.24	102.43	8.486E+05	0.54	0.41
Spring 6	3965.3	355.42	43.467	8.149E+05	0.22	0.18
Shuttles	3965.3	3818	5091.2	7.474E+04	2.37	20.59
Total	. . .	. . .	. . .	. . .	**98.88**	**96.53**

Table 12 Q_{TED}-by-domain QMG Design 4

Design 4 (1.4 million)	Frequency (Hz)	Elastic energy (∭solid.Ws) (J/m)	TED (∭solid.Qted) (W/m)	Q due to TED	% Energy stored	% Energy dissipated
QMG	3067.8	1.48E+05	13474	8.447E+05	. . .	. . .
Spring 1	3067.8	89380	6153.2	1.120E+06	60.55	45.67
Spring 2	3067.8	45870	3323.2	1.064E+06	31.07	24.66
Spring 3	3067.8	7939.5	1232.3	4.968E+05	5.38	9.15
Spring 4	3067.8	183.79	14.811	9.568E+05	0.12	0.11
Shuttles	3067.8	2071.7	2256.6	7.078E+04	1.40	16.75
Spring 6	3067.8	289.16	23.585	9.453E+05	0.20	0.18
Total	. . .	. . .	. . .	. . .	**98.72**	**96.51**

3.3.3 Impact of Including Etch-Holes in Shuttle

Since the shuttles were having a large impact on the calculated quality factor in our TED simulations, we wanted to better-represent the actual device by adding in the release etch holes (Fig. 27), which previously had been ignored for model simplicity. As evident by comparing Tables 12 and 13, with or without the etch holes the shuttle is a location of substantial energy loss.

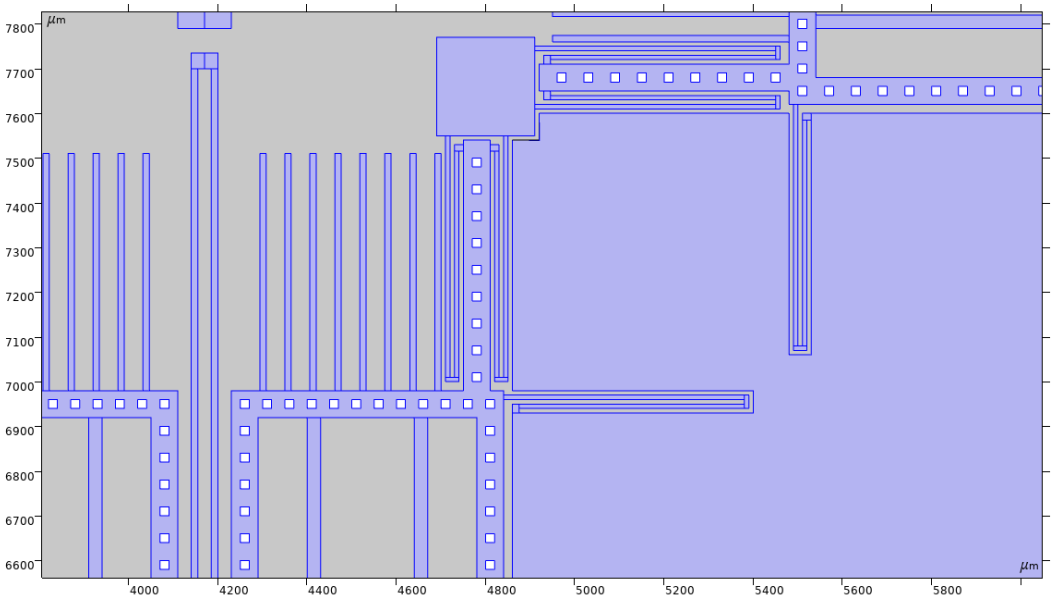

Fig. 27 Etch holes added to the shuttle

Table 13 Q_{TED}-by-domain QMG Design 4 with shuttle holes

Design 4 (1.4 million)	Frequency (Hz)	Elastic energy (∭solid.Ws) (J/m)	TED (∭solid.Qted) (W/m)	Q due to TED	% Energy stored	% Energy dissipated
QMG	3079.4	1.39E+05	13563	7.935E+05	. . .	. . .
Spring 1	3079.4	84099	5839.6	1.115E+06	60.48	43.06
Spring 2	3079.4	43189	3156.9	1.059E+06	31.06	23.28
Spring 3	3079.4	7480.2	1169.4	4.951E+05	5.38	8.62
Spring 4	3079.4	173.21	14.179	9.454E+05	0.12	0.10
Shuttles w/ holes	3079.4	2069.3	2914.6	5.495E+04	1.49	21.49
Spring 6	3079.4	272.21	22.351	9.426E+05	0.20	0.16
Total	. . .	. . .	. . .	. . .	**98.73**	**96.71**

3.3.4 Comparison to Experimental Results and Zener Model

The COMSOL TED simulation results are compared to experimentally measured quality factors in Tables 14–17. We take the results of the 2-D COMSOL simulations and scale the frequency and quality factor as described in Section 3.2.3

to extrapolate our 2-D simulations to expected 3-D results. The 10 μm silicon beam Zener model quality factor is provided for both the experimental and COMSOL frequencies.

Table 14 COMSOL Q_{TED} vs. experimental Q, Design 1

Method	Frequency (Hz)	Q	F*Q
Experimental	1888.6	8.50E+05	1.61E+09
COMSOL 2-D	3298.9	7.91E+05	2.61E+09
COMSOL 3-D extrapolation	3232.922	1.09E+06	3.52E+09
Zener (10 μm)	1888.6	3.21E+06	6.06E+09
Zener (10 μm)	3298.9	1.84E+06	6.06E+09

Table 15 COMSOL Q_{TED} vs. experimental Q, Design 2

Method	Frequency (Hz)	Q	F*Q
Experimental	2750	1.24E+06	3.42E+09
COMSOL 2-D	3410.8	7.67E+05	2.61E+09
COMSOL 3-D extrapolation	3342.584	1.05E+06	3.53E+09
Zener 10 μm	2750.074	2.21E+06	6.06E+09
Zener 10 μm	3410.8	1.78E+06	6.06E+09

Table 16 COMSOL Q_{TED} vs. experimental Q, Design 3

Method	Frequency (Hz)	Q	F*Q
Experimental	3157	8.03E+05	2.54E+09
COMSOL 2-D	3965.3	6.51E+05	2.58E+09
COMSOL 3-D extrapolation	3885.994	8.95E+05	3.48E+09
Zener 10 μm	3156.349	1.92E+06	6.06E+09
Zener 10 μm	3965.3	1.53E+06	6.06E+09

Table 17 COMSOL Q_{TED} vs. experimental Q, Design 4

Method	Frequency (Hz)	Q	F*Q
Experimental	1959.9	1.42E+06	2.79E+09
COMSOL 2-D	3067.8	8.45E+05	2.59E+09
COMSOL 3-D extrapolation	3006.444	1.16E+06	3.50E+09
Zener 10 μm	1959.489	3.09E+06	6.06E+09
Zener 10 μm	3067.8	1.98E+06	6.06E+09

There is a substantial difference between the modeled frequency of operation and the experimental frequency for some of the designs. Possible explanations for this include dimensional changes during the fabrication process or COMSOL model parameters that we can fit better after accumulating more data. Previous devices

had issues with the resist exposure, and after improving the lithography recent devices have frequencies that shift upward around 20%–25%.

Looking at the F*Q metric, consistency with what one would predict exists as the 3-D COMSOL extrapolation for F*Q falls between the experimental values (where other damping is present) and the 10 µm Zener model (the QMG's smallest dimension is 10 µm, therefore we should expect the Zener model to be an upper bound).

3.4 Modifying Springs (Fillets, Chamfers, Corner Bites, Changing Widths, Shuttle Connection)

Since spring 1 is the most active component of the QMG in terms of energy storage and heat loss, we explored how modifying its geometry impacts Q_{TED} performance. This geometry modification could be considered something we design in the future or the non-idealities associated with the fabrication process (for example, imperfect corners). Additionally, the connection from spring 1 to the shuttle was limiting Q_{TED} so we looked at modifying that connection's dimensions.

3.4.1 Spring 1: Fillets, Chamfers, and Corner Bites

The corners of spring 1 were modified with different sizes of fillets, chamfers, and corner bites. As expected, the fillets and chamfers spread out where the solid.Qted heat source was generated and lowered the highest wattage measured (Fig. 28).

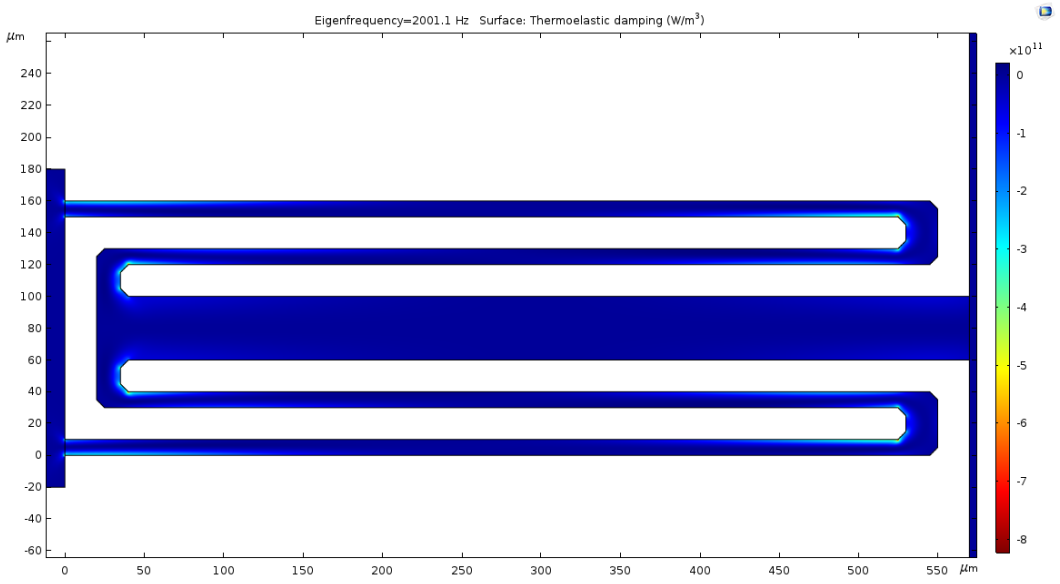

Fig. 28 Spring 1 with a 5 µm corner chamfer

However, the impact this corner modification had on the quality factor was minimal and made the quality factor worse (Table 18).

Table 18 Corner modifications to spring 1

Design	Center density (kg/m^3)	Frequency (Hz)	Q	F*Q
Original	2330	2253.0	1.5272E+06	3.441E+09
Original	3455	2001.1	1.7171E+06	3.436E+09
Fillet 5 µm	2330	2279.7	1.4242E+06	3.247E+09
Fillet 5 µm	3580	2001.5	1.6155E+06	3.233E+09
Chamfer 2 µm	2330	2267.0	1.4397E+06	3.264E+09
Chamfer 2 µm	3520	2001.4	1.6246E+06	3.251E+09
Fillet 10 µm	2330	2316.3	1.4470E+06	3.352E+09
Fillet 10 µm	3760	2000.9	1.6708E+06	3.343E+09
Chamfer 5 µm	2330	2296.9	1.4708E+06	3.378E+09
Chamfer 5 µm	3665	2001.1	1.6847E+06	3.371E+09

After determining that distributing the stress and strain throughout the corner led to a slightly worse Q, we tried to localize the stress and strain even more in the corners by adding a 1 µm corner bite (Fig. 29).

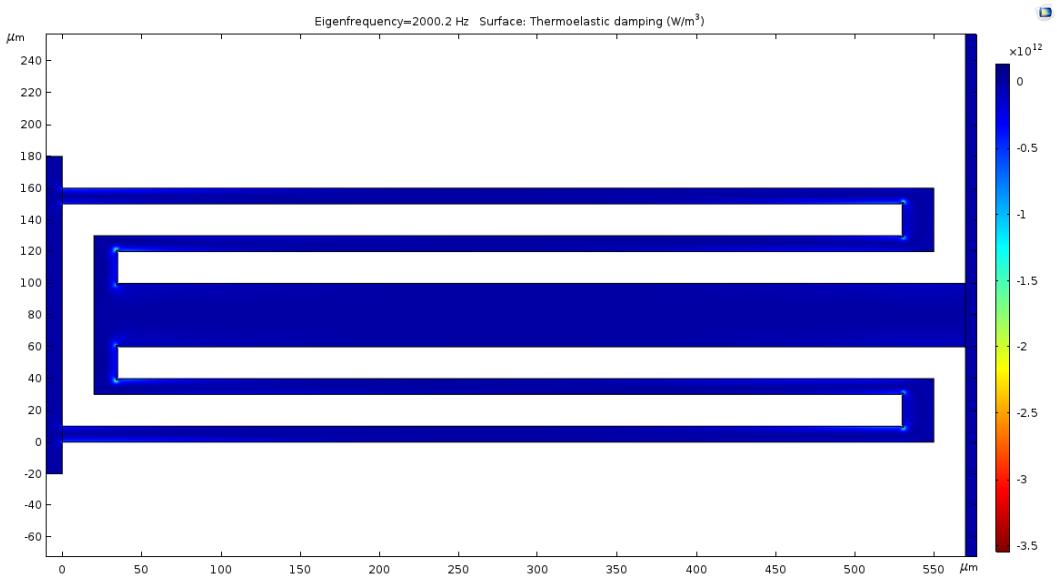

Fig. 29 Spring 1 with a 1 µm corner bite

While the corner bite did improve the quality factor (Table 19), it was only by approximately 1% or 2%.

Table 19 Impact of triangular corner bites spring 1

Design	Center density (kg/m^3)	Frequency (Hz)	Q	F*Q
Original	2330	2253.0	1.5272E+06	3.441E+09
Original	3455	2001.1	1.7171E+06	3.436E+09
1 µm triangle bites	2330	2223.2	1.5707E+06	3.492E+09
1 µm triangle bites	3320	2000.2	1.7440E+06	3.488E+09

3.4.2 Changing Spring Width

Q_{TED} should be proportional to $\frac{1}{W^2}$, however as shown in Table 20, the performance increase seen by decreasing the spring width is much less. The reason for this is the connection to the shuttle that needs to be stiffened (Fig. 30).

Table 20 Impact of scaling dimensions of spring 1, but not changing the shuttle connection

Design	Center density (kg/m^3)	Frequency (Hz)	Q	F*Q
Original	2330	2253.0	1.53E+06	3.44E+09
Original	3455	2001.1	1.72E+06	3.44E+09
8 µm width	2330	2472.7	1.75E+06	4.33E+09
8 µm width	4550	1999.7	2.1488E+06	4.297E+09
6 µm width	2330	2241.1	2.6156E+06	5.862E+09
6 µm width	3400	2000.4	2.9186E+06	5.838E+09
4 µm width	2330	2302.3	2.5843E+06	5.950E+09
4 µm width	3700	1998.6	2.9658E+06	5.927E+09

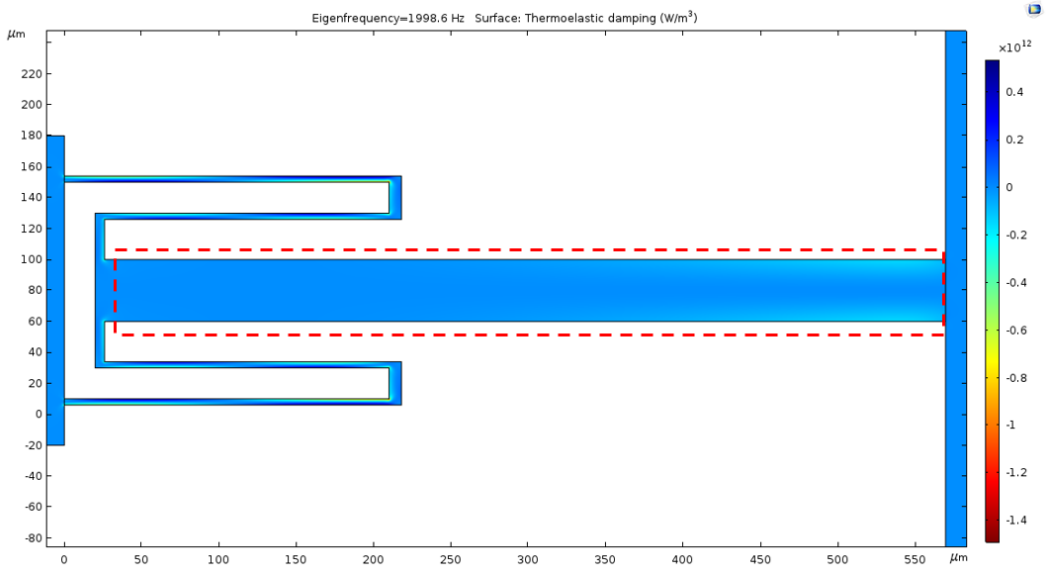

Fig. 30 Spring 1 scaled, but the shuttle connection unchanged

3.4.3 Shuttle Connection Impact

By changing the shuttle connection length as well as scaling the dimensions of the spring (Fig. 31), a relationship close to $Q_{TED} \propto \frac{1}{W^2}$ is observed (Table 21).

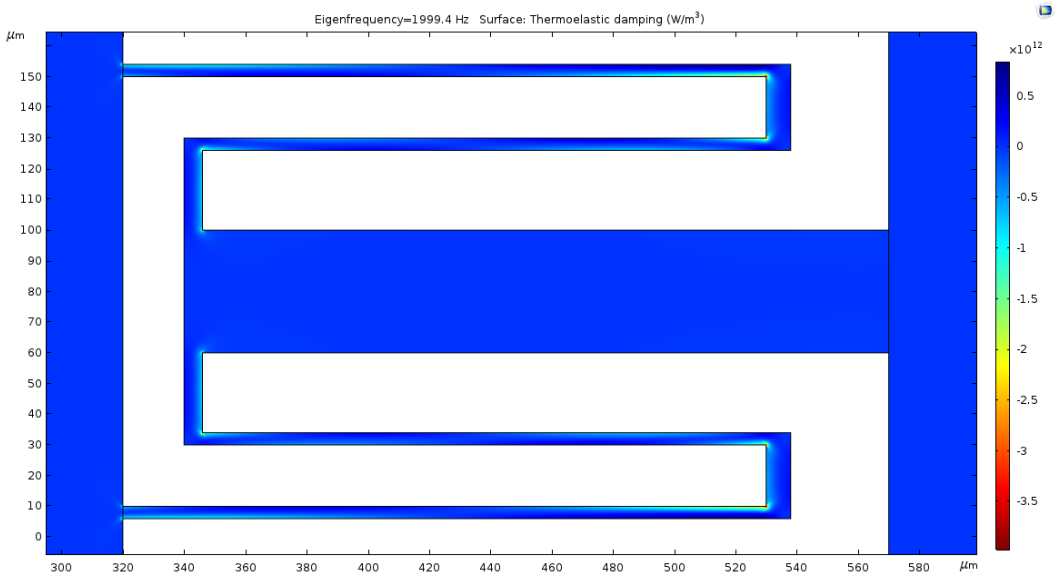

Fig. 31 Spring 1 scaled, with the shuttle connection length scaled as well

Table 21 Impact of scaling dimensions of spring 1, and the shuttle connection length

Design	Center density (kg/m³)	Frequency (Hz)	Q	F*Q
Original	2330	2253.0	1.53E+06	3.44E+09
Original	3455	2001.1	1.717E+06	3.44E+09
8 µm width	2330	2491.3	2.105E+06	5.24E+09
8 µm width	4650	2002.5	2.609E+06	5.22E+09
6 µm width	2330	2269.7	4.280E+06	9.71E+09
6 µm width	3525	2001.4	4.844E+06	9.70E+09
4 µm width	2330	2354.3	9.322E+06	2.20E+10
4 µm width	3940	1999.4	1.095E+07	2.19E+10

Key takeaways were as follows:

- Spring 1 stores the most energy, so it was investigated for potential improvements using the spring-mass-spring setup.
- Modifying corners of springs with fillets, chamfers, and so forth did not change device performance in an appreciable manner.
- The decrease in the width of spring 1 is not fully fruitful unless the shuttle connection is shortened/stiffened as well. This connection needs to be optimized and investigated further to optimize Q_{TED} performance.

3.5 DRG Modeling

Unlike the QMG, the DRG cannot be easily subdivided into unique domains so only the eigenfrequency Q_{TED} was investigated.

3.5.1 Simulation Setup

The DRG simulation requires only a single anchor point (Fig. 32).

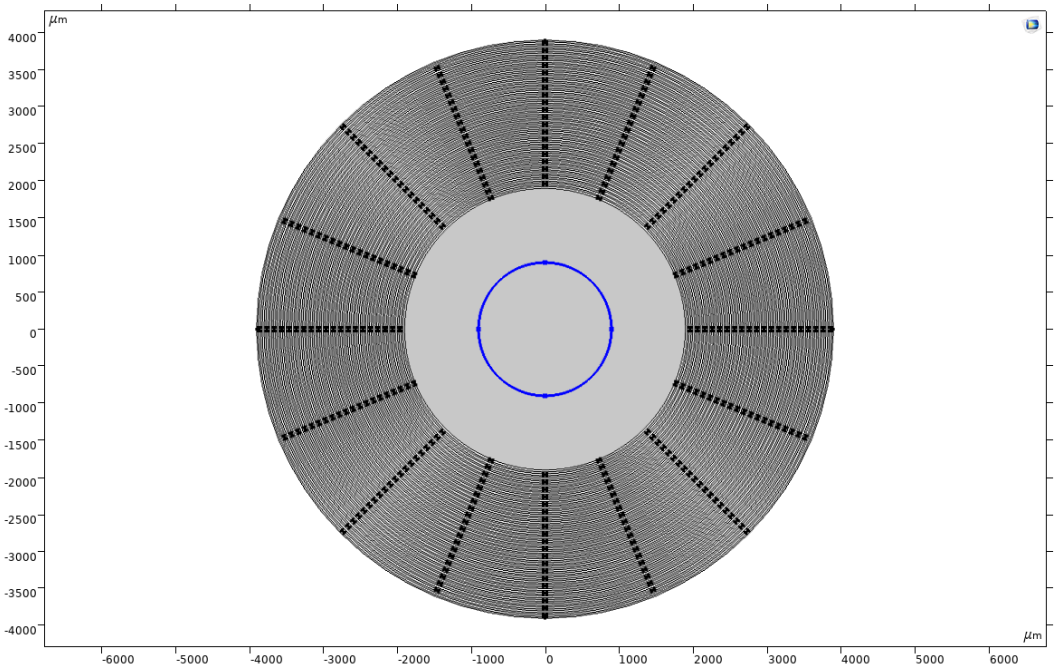

Fig. 32 DRG anchor and isothermal boundary condition location

A simple mesh refinement study was performed to find an acceptable trade-off between mesh density and simulation time (Table 22).

Table 22 COMSOL DRG mesh refinement

Mesh definition	Domain elements	Frequency (Hz)	Q
Physics: coarser	183932	14771	52835
Physics: coarse	244476	14658	51965
User: max 10 µm	473154	14630	48307
User: max 8 µm	824988	14626	46919

All results shown in this report use a user-defined mesh of 8 µm maximum for the springs.

3.5.2 (100) and (111) Results

The simulated results of a DRG using (100) and (111) silicon are listed in Table 23. Tables 24 and 25 compare the simulated results with experimental measurements and the Zener model. Figures 33 and 34 show the corresponding mode-shapes.

Table 23 COMSOL Q_{TED} results: DRG

Mode	Frequency (Hz)	Q	F*Q
n = 3 (100)	14606	47107	6.88E+08
n = 3 (100)	14606	47110	6.88E+08
n = 2 (111)	12351	58682	7.25E+08
n = 2 (111)	12351	58680	7.25E+08

Table 24 COMSOL Q_{TED} vs. experimental Q, DRG (100), n = 3

Method	Frequency (Hz)	Q	F*Q
Experimental	13586.1	6.04E+04	8.21E+08
Experimental	13308.3	6.02E+04	8.01E+08
COMSOL 2-D	14606	4.71E+04	6.88E+08
COMSOL 2-D	14606	4.71E+04	6.88E+08
COMSOL 3-D extrapolation	14313.88	6.48E+04	9.29E+08
COMSOL 3-D extrapolation	14313.88	6.48E+04	9.29E+08
Zener 25µm	13440.99	7.25E+04	9.75E+08
Zener 25µm	14606	6.68E+04	9.75E+08

Table 25 COMSOL Q_{TED} vs. Zener Q, DRG (111), n = 2

Method	Frequency (Hz)	Q	F*Q
COMSOL 2-D	12351	58682	7.25E+08
COMSOL 2-D	12351	58680	7.25E+08
COMSOL 3-D extrapolation	12103.98	77753	9.41E+08
COMSOL 3-D extrapolation	12103.98	77751	9.41E+08
Zener 25µm	12351	78900	9.75E+08

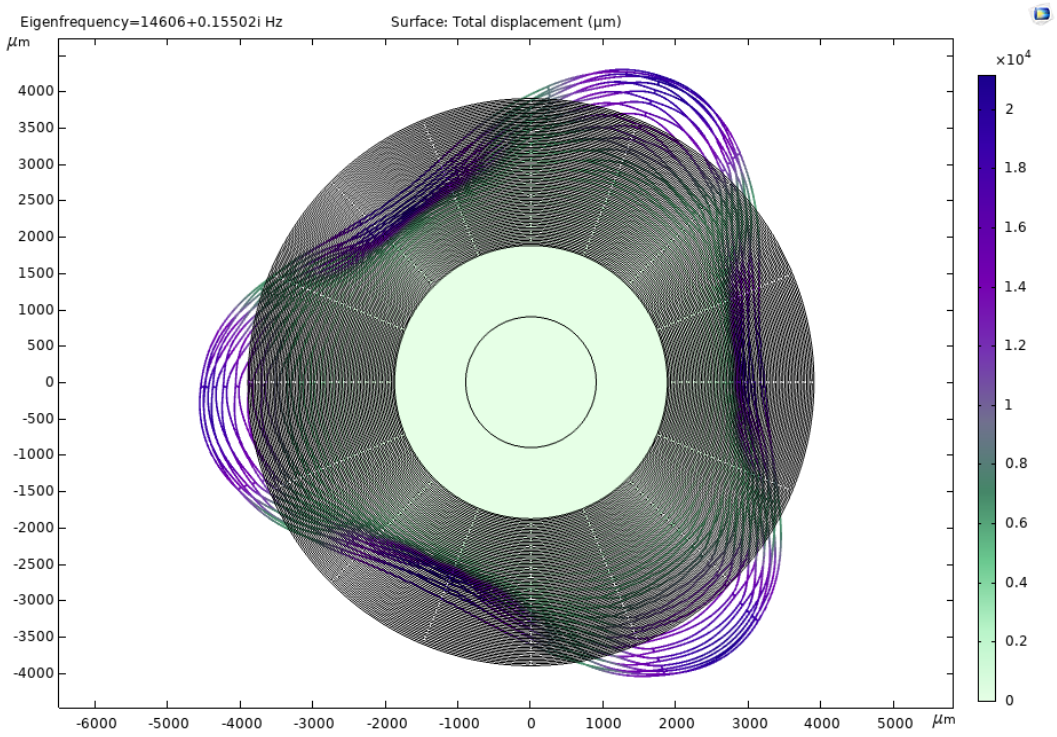

Fig. 33 DRG (100) operating in the n = 3 mode

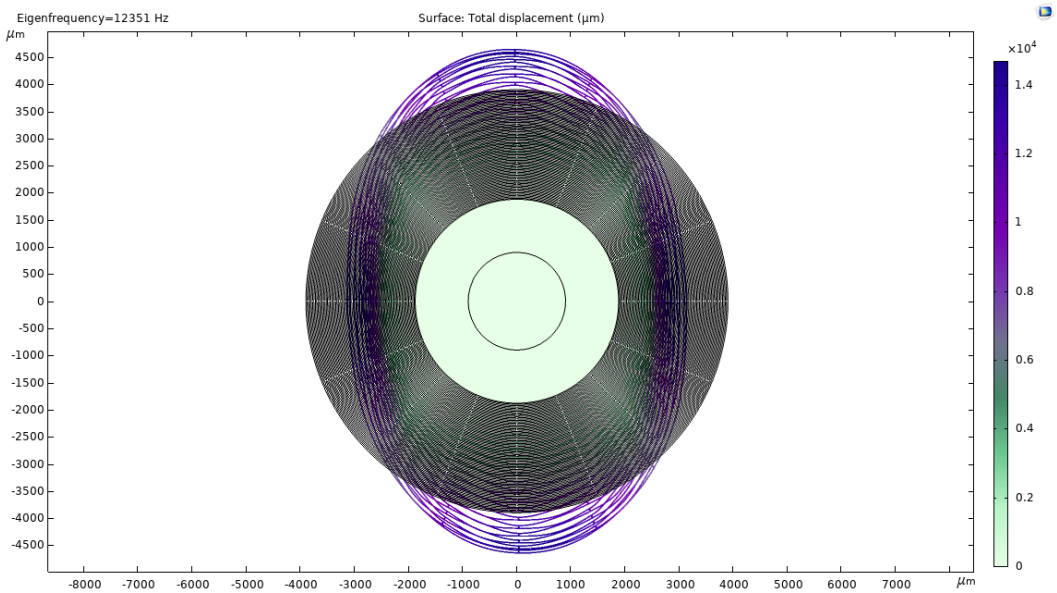

Fig. 34 DRG (111) operating in the n = 2 mode

Once again, the COMSOL F*Q 3-D extrapolation falls between the experimental results and the Zener Q_{TED} model. However, unlike the QMG, the results for the DRG are much closer together. From a dimensional point of view this makes sense as the DRG has a singular spring size and shape, whereas the QMG has multiple differently sized components. The DRG is also less susceptible to fabrication imperfections because the springs are 25 μm wide, compared to 10 μm for the QMG.

We do not have in-house data for DRG performance on (111) silicon; however, as expected, the COMSOL simulation gives an F*Q product just below the Zener model's estimate.

4. Conclusions

4.1 Key Achievements

The key achievements in this work are as follows:

- Analytical models for TED scripted to make informed design-space decisions.
- Method developed to model TED in QMG designs using COMSOL.
- Modeled QMG TED performance compared with experimental results and analytical models.
- Method developed to model TED performance of individual components of QMG.
- Low-Q_{TED} areas of the QMG design highlighted, along with potential ways to improve device performance.
- COMSOL TED model applied to the DRG and other resonator designs.

4.2 Other Simulations and Future Work

Using components of the QMG (springs 1, 3, 5, and the shuttles), a simplified resonator (Fig. 35) with two masses and one vibrational axis was designed.

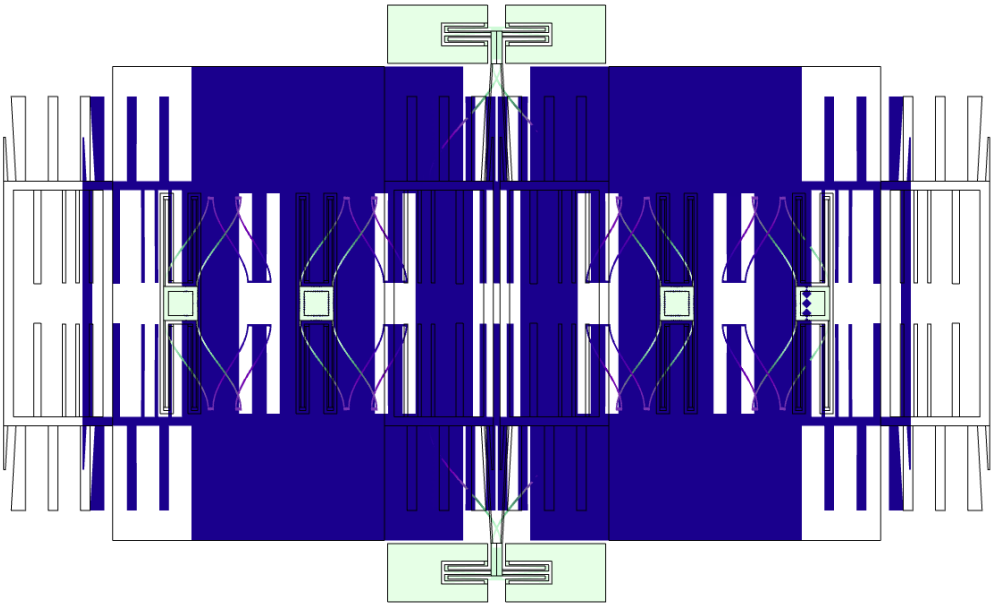

Fig. 35 Simple resonator mode-shape

The main purpose of this “Simple Resonator” is to investigate the fabrication sources of frequency mismatch between orthogonal modes of the QMG. This design will also help with validation and improvement of the TED modeling.

Multiples designs of the Simple Resonator with different spring and connection widths have been made in CAD and simulated in COMSOL for Q_{TED}. Once fabricated, experimental results of the Simple Resonator along with more QMG and DRG performance data can provide feedback to improve the COMSOL TED modeling process and optimize the QMG connections shown in Fig. 36.

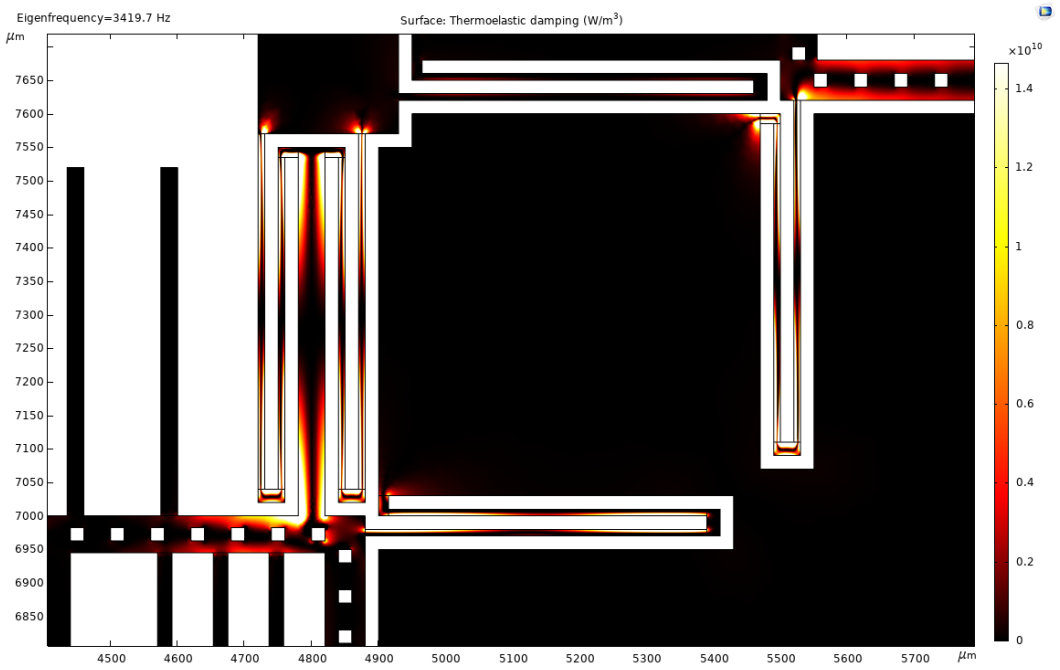

Fig. 36 Location of the dominant TED losses in QMG designs and future design optimization

The most straightforward way to improve Q_{TED} is to use thinner springs. However, there is fundamental trade-off involved when decreasing spring dimensions as it will increase frequency splitting. Additionally, as mentioned previously, the connection to the shuttles needs to be improved for the decreasing spring width to be fully effective. Like the work done by Candler et al., we could strategically place slots or other features to disrupt the heat flow in areas with larger dimensions and improve Q_{TED}.[15] Results from the Simple Resonator devices will provide information about what dimensions are feasible from a fabrication perspective and the trade-off with frequency splitting. Using that data, parametric simulations incorporating etch-hole dimensions and placement, spring dimensions, beam dimensions, and shuttle dimensions can be performed to find an optimized Q_{TED} design.

5. References

1. Leland RP. Mechanical-thermal noise in MEMS gyroscopes. IEEE Sens J. 2005;5:493–500.
2. Zener C. Internal friction in solids II. General theory of thermoelastic internal friction. Phys Rev. 1938;53:90–99.
3. Lifshitz R, Roukes M. Thermoelastic damping in micro- and nanomechanical systems. Phys Rev B Condens Matter Mater Phys. 2000;61:5600–5609.
4. Prabhakar S, Vengallatore S. Theory of thermoelastic damping in micromechanical resonators with two-dimensional heat conduction. J Microelectromechanical Syst. 2008;17:494–502.
5. Rodriguez J, Chandorkar SA, Watson CA, Glaze GM, Ahn CH, Ng EJ, Yang Y, Kenny TW. Direct detection of Akhiezer damping in a silicon MEMS resonator. Sci Rep. 2019;9:1–10.
6. Knight RR, Devoe DD, Polcawich RG, Pulskamp JS, Power BK. Micro-torr vacuum packaging of gettered ceramic chip carriers. Proceedings of INERTIAL 2019 - 6th IEEE International Symposium on Inertial Sensors and Systems, Proceedings; 2019. Institute of Electrical and Electronics Engineers Inc. doi:10.1109/ISISS.2019.8739428.
7. Zotov SA, Simon BR, Prikhodko IP, Trusov AA, Shkel AM. Quality factor maximization through dynamic balancing of tuning fork resonator. IEEE Sens J. 2014;14(2706–2714).
8. MATLAB. Release 2019a. The Mathworks, Inc.; 2019.
9. Thermoelastic damping in a MEMS resonator. Application ID 1439. COMSOL; n.d. [accessed 2019 July 11]. https://www.comsol.com/model/thermoelastic-damping-in-a-mems-resonator-1439.
10. Hopcroft MA, Nix WD, Kenny TW. What is the Young's modulus of silicon? J Microelectromechanical Syst. 2010;19:229–238.
11. Qin Z, Gao Y, Jia J, Ding X, Huang L, Li H. The effect of the anisotropy of single crystal silicon on the frequency split of vibrating ring gyroscopes. Micromachines. 2019;10.
12. MEMS module user's guide 5.5. COMSOL; n.d. [accessed 2021 June 29]. p. 216–225. https://doc.comsol.com/5.5/doc/com.comsol.help.mems/MEMSModuleUsersGuide.pdf

13. Watanabe H, Yamada N, Okaji M. Linear thermal expansion coefficient of silicon from 293 to 1000 K. Int J Thermophys. 2004;25:221–236.

14. Middelmann T, Walkov A, Bartl G, Schödel R. Thermal expansion coefficient of single-crystal silicon from 7 K to 293 K. Phys Rev B Condens Matter Mater Phys. 2015;92:174113.

15. Candler RN, Duwel A, Varghese M, Chandorkar S, Hopcroft M, Park W-T, Kim B, Yama G, Partridge A, Lutz M, et al. Impact of geometry on thermoelastic dissipation in micromechanical resonant beams. J Microelectromechanical Syst. 2006;15:927–934.

List of Symbols, Abbreviations, and Acronyms

2-D	2-dimensional
3-D	3-dimensional
ARL	Army Research Laboratory
ARW	angle of random walk
CAD	computer-aided design
CTE	coefficient of thermal expansion
CVG	Coriolis vibratory gyroscope
DEVCOM	US Army Combat Capabilities Development Command
DRG	disk resonator gyroscope
GPS	global positioning system
MEMS	microelectromechanical system
PC	personal computer
PNT	positioning, navigation, and timing
Q	quality factor
QMG	quadruple-mass gyroscope
RAM	random access memory
TED	thermoelastic damping

1 (PDF)	DEFENSE TECHNICAL INFORMATION CTR DTIC OCA
1 (PDF)	DEVCOM ARL FCDD RLD DCI TECH LIB
5 (PDF)	DEVCOM ARL FCDD RLS SA A MAZZONI R RUDY R KNIGHT J PULSKAMP W ALBERTS